MEK-SHP2 inhibition prevents tibial pseudarthrosis caused by *NF1* loss in Schwann cells and skeletal stem/progenitor cells

Supplemental material

Supplementary Material and Methods

DNA extraction and *NF1* genotyping of samples from patients with CPT

Collected tissue samples were snap-frozen in liquid nitrogen and stored at -80°C until processing for DNA extraction. Tissue disruption was performed using TissueLyser system (Qiagen). DNA was isolated from disrupted tissues or primary culture of periosteal cells using standard proteinase K digestion followed by phenol-chloroform extraction. DNA concentrations were assessed by spectrophotometry using Qubit 2.0 Fluorometer (ThermoFisher Scientific). Sequencing was performed at the next-generation sequencing (NGS) facility of Cochin Hospital, Paris. *NF1* genotyping was performed using targeted NGS allowing *NF1* point mutations and copy number variation detection, as previously described *(57)*. Briefly, targeted regions were sequenced using Ion Torrent PGM/S5 or Illumina MiSeq technologies after multiplex PCR amplification including the coding exons and the flanking intronic regions (25 bp) of *NF1* gene and *SPRED1* gene as copy number reference. Sequence alignment was performed with the Torrent Mapping Alignment Program (TMAP, Ion Torrent, Thermo Fisher Scientific) or BWA Aligner (Illumina). Aligned reads from BAM files were visualized using the Integrative Genomics Viewer v2.3 from the Broad Institute (Cambridge, MA, USA). SNVs and short Indels were annotated, ranked, and interpreted using the Polydiag suite (Bioinformatics Department, Paris-Descartes University). Variant allele frequency (VAF) was calculated by dividing alternative/WT alleles read depths. Structural variants (single and multi-exon deletion/duplication) were also investigated. *NF1* amplicon reads were first internally normalized by *SPRED1* amplicon reads. Subsequently, normalized reads obtained for each amplicon of a sample were then divided by the average normalized reads of control samples for the corresponding amplicon. Copy number ratios of 0,9 to 1,1 allowed the exclusion of a deletion. Copy number ratios under 0.8 were considered deleted. *NF1* 1st and 2nd hits were determined based on VAF, except for patients P3 and P15, where equivalent VAF of the 2 hits did not allow identification of the mutational chronology.

***NF1* variant quantification using droplet digital PCR**

To identify the cell types carrying *NF1* biallelic inactivation, we performed droplet digital PCR on sorted periosteal cell populations of patient P15. Freshly collected periosteum was washed in PBS, minced using scissors and digested 1 hour at 37°C in PBS with 3mg/ml of Collagenase B (C6885, Merck), 4mg/ml of Dispase (D4693, Merck) and 100U/mL of DNAse I (WOLS02007, Serlabo, France). After

centrifugation, cells were incubated with antibodies listed in Table S2. Immune cells, endothelial cells, SSPCs and Schwann cells were sorted using Influx Cell Sorter. DNA was extracted from the sorted cells using the Qiagen QIAamp DNA Micro kit (56304, Qiagen) and droplet digital PCR was performed using the QX100™ Droplet Digital™ PCR System (BioRad) according to the manufacturer's instructions. Duplex PCR of NF1 WT c.574C / mutant c.574T and NF1 WT c.5839C / mutant c.5839T alleles were carried out in duplicates by using PCR primers and probes (Bio-Rad ID dmDS626740718/c.574C>T and dmDS133057715/c5839C>T).

***NF1* transcript analysis**

When targeted NGS performed on genomic DNA did not reveal any pathogenic variant in the *NF1* coding sequence (patients 8, 10, 11, 16, 17), RNA samples (2 µg) extracted from PA and IC pSSPCs were reverse transcribed using 50 units of MultiScribe™ Reverse Transcriptase, 40 units of RNase Inhibitor and 1.5 mM pd(N)6 Random hexamer 5'phosphate (Thermo Fisher Scientific). The samples were incubated at 20°C for 10 min and 37°C for 120 min. Reverse transcriptase was then inactivated by heating at 85°C for 5 min and cooling at 5°C for 5 min. The full cDNA was then amplified in 8 overlapping fragments further sequenced as already described *(58)*.

Mouse tibial fracture

For all surgical procedures, mice were anesthetized with an intraperitoneal injection of Ketamine (50 mg/mL) and Medetomidine (1 mg/kg) and received a subcutaneous injection of Buprenorphine (0.1 mg/kg) for analgesia. Mice were kept on a 37°C heating pad during anesthesia. For phenotypic analyses, closed non-stabilized fractures were performed in mid-diaphysis of the right tibia by three-point bending *(12)*. Briefly, the tibia was placed on a fracture jig, and a 470g weight was dropped from 11.5 cm to induce the fracture. For cell and tissue grafting, open non-stabilized tibial fractures were performed *(12)*. The right hindlimb was shaved and sanitized. The skin was incised to expose the tibia and osteotomy was performed in the mid-diaphysis by cutting the bone. To provide partial stabilization (semi-stabilized fracture in Fig. S7), an intramedullary pin was inserted in the medullary cavity after inducing the fracture as previously described in *(51)*. The wound was sutured, the mice were revived with an intraperitoneal injection of atipamezole (1 mg/kg) and received two additional analgesic injections in the 24 hours following surgery.

Tissue transplantation at fracture site

Tissue transplantation was performed as previously described *(12, 51)*. Grafted tissues were collected from *Prss56^{Cre}, R26^{tdTom}, Nf1$^{+/+}$* or *Prss56^{Cre}, R26^{tdTom}, Nf1$^{fl/fl}$* mice. For periosteum transplantation, a piece of cortical bone was collected from the anterior-proximal area of the donor tibia. The endosteum and bone marrow were removed. A cortical defect was performed on the anterior-proximal surface of the tibia of the host, adjacent to a fracture site. The graft was placed within the cortical defect. The muscle was sutured over the defect to hold the graft in position. For muscle transplantation, EDL (Extensor digitorum longus) muscle was dissected from tendon to tendon and grafted on the anterior surface of the tibia of the host wild-type mice. The grafted EDL was sutured to the host patellar and peroneus muscle tendons with non-resorbable sutures (12051-08, Fine Science Tool, Germany). After tissue grafting, a non-stabilized fracture was induced as described above.

Selumetinib and SHP099 in vivo treatment

Prss56-Nf1$^{fl/-}$ were treated by daily oral gavage of 25 mg/kg of selumetinib (HY-50706, Clinisciences), 50mg/kg of SHP099 (HY-100388, Clinisciences), or the combination of selumetinib and SHP099. Control mice were treated with the vehicle, composed of 0,5% methylcellulose and 0,2% Tween80.

TGFβ blocking antibody treatment

InVivoMAb antimouse/human/rat/monkey/hamster/canine/bovine TGF-β, Clone 1D11 (BX-BE0057) was purchased from Euromedex. Mice were treated at days 5, 8 and 11 post-fracture by intraperitoneal injection of 5 mg/kg of TGF-β blocking antibody diluted in PBS. Control mice were treated with 5 mg/kg InVivoMAb mouse IgG1 isotype control antibody (BX-BE0083, Euromedex).

MicroCT and bone union scoring

Callus samples or tibias were scanned at the Small Animal Platform of Paris Cité University (EA2496, Paris Cité) using X-ray micro- CT device (Quantum FXCaliper, Life Sciences, Perkin Elmer, Waltham, MA) with the X-ray source at 90 kV and 160 µA. A 10 mm field of view and 20 µm voxel size was used. Images were processed using Horos software. Bone parameters (cortical porosity and bone volume/ total volume (BV/TV)) were determined on 1mm sections using CTan software v1.17.7.2 (Bruker,

Hamburg, Germany). Tibial length and bowing were determined on all tibia microCT scans using Horos software. Callus bridging was determined in sagittal and longitudinal axes and the number of bridged sides was evaluated. A callus bridged in 3 or 4 sides was considered as union, 2 sides as semi-union, and 1 or 0 side as nonunion *(51)*. For *Prx1-Nf1* KO mice, bone union was determined on histological section.

Tissue sample processing and histology

Human periosteum samples were fixed in ice-cold 4% PFA (sc-281692, CliniSciences) for 24 hours, before cryo-embedding or paraffin embedding. Mouse samples were processed as previously described *(12)*. Mice were euthanized and the uninjured or fractured tibias were collected and fixed in ice-cold 4% paraformaldehyde for 4 or 24 hours upon agitation. Samples were decalcified in 19% EDTA (EU00084, Euromedex) for 1 to 3 weeks at 4°C under constant agitation, placed in 30% sucrose (200-301-B, Euromedex) for 24h before embedding in cryoprotectant. Samples were cryosectioned throughout the entire callus in 10µm thick sections. All thirtieth sections were defrosted, rehydrated and stained with Picrosirius, Masson's Trichrome or Safranin'O staining. After staining, sections were dehydrated with successive ethanol and NeoClear incubations. Slides were mounted using NeoMount medium (1.09016.0100, VWR, USA). Stained sections were pictured using a Zeiss Imager D1 AX10 light microscope (Carl Zeiss Microscopy GmbH).

Picrosirius staining (PS)

Sections were stained in PicroSirius solution, 0.1% of Direct Red 80 (43665-25G, Merck) in picric acid (80456, Merck) for 2 hours protected from light.

Masson's trichrome staining (TC)

Sections were first stained in Harris hematoxylin diluted ½ (F/C0283, MMFrance) for 5 min, washed in tap water for 5 min, stained with Red Mallory for 10 min, washed for 5 min and then placed 10 min in phosphomolybdic acid 1% (HT153, Merck). Finally, sections were stained 20 min in light green (720-0335, VWR) and fixed in 1% acetic acid.

Safranin'O staining (SO)

Sections were stained with Weigert's solution for 5 min, rinsed in running tap water for 3 min and stained with 0.02% Fast Green for 30 seconds (F7252, Merck), followed by 1% acetic acid for 30 seconds and Safranin'O solution for 45 min (S2255, Merck).

Histomorphometric analyses

Histomorphometric analyses was performed on every thirtieth section throughout the entire callus as described in *(12)*. Areas of callus, cartilage, bone and fibrosis were determined using ZEN software v1.1.2.0 (Carl Zeiss Microscopy GmbH) on SO, TC and PS staining respectively. Volumes were calculated using the formula: $volume = \frac{1}{3}h\sum_{1}^{n-1}(A_i + A_{i+1} + \sqrt{A_i * A_{i+1}})$ with A_i and A_{i+1} being the areas of callus, cartilage, bone and fibrosis in following sections, h was the distance between Ai and Ai + 1 and equal to 300 µm and n the total number of sections analyzed in the sample.

Immunostaining

Cryosections were defrosted at room temperature protected from light and rehydrated in PBS. Paraffin sections were deparaffinized by successive Neo-Clear and alcohol incubations and rehydrated in PBS. For phospho-ERK (pERK), OSX, SOX10 and KU80 immunofluorescence, an antigen retrieval step was performed by incubating the slides in citrate buffer at 95°C for 20 min, followed by 20 min at 4°C. Sections were incubated 1 hour at room temperature in 5% serum, 0.25% Triton PBS before incubation with primary antibodies listed in the Table S3 overnight at 4°C. Secondary antibody incubation was performed at room temperature for 1 hour. Slides were mounted with Fluoromount-G mounting medium with DAPI (00-4959-52, Life Technologies). Sections of paraffine-embedded human periosteum samples were deparaffinized, and incubated with H2O2 for 5 minutes, 0.1% trypsin for 30 minutes, 0.1M Glycine for 1 minutes, 5% powdered milk for 10 minutes, 0.1% ovalbumine for 10 minutes and 5% Normal Goat Serum for 30 minutes prior to antibodies incubation. All immunostainings were validated using positive controls.

Quantification of fluorescent signal

Quantification of tdTom signal in the callus. The surface of tdTom signal in the callus, cartilage, bone and fibrosis of *Prss56-Nf1*$^{+/+}$ or *Prss56-Nf1*$^{fl/fl}$ mice was measured on three central-callus sections 300

µm apart as described in *(12)*. The sections were pictured using Zeiss Imager D1 AX10 microscope and tdTom surface was measured using Zen Software.

Percentage of tdTom chondrocytes, osteoblasts, fibroblasts, and proliferating cells. The number of SOX9, OSX and *Postn* positive cells and tdTom+ SOX9, OSX, *Postn,* KI67 positive cells was determined using Qupath.

Quantification of tissue or cell graft contribution. For graft contribution, tdTom or GFP signal was measured every 300 µm through the entire callus. The tdTom or GFP signal was pictured using Zeiss Imager D1 AX10 microscope and tdTom or GFP surface was measured using Zen Software.

Quantification of pERK+ and pSMAD2+ cells. The percentage of phospho-ERK+ and phosho-SMAD2+ cells was calculated by the number of pERK+ or pSMAD2+ cells compared to the number of DAPI+ nuclei using QuPath. For each sample, the percentage of pERK+ and pSMAD2+ cells were determined by the mean of 2 sections 300µm apart. For each section, the number of positive cells was determined in 3 areas of the callus. For co-immunostaining on human periosteum sections, the number of CD90+, SOX10+, CD31+, CD68+ and aSMA+ cells was counted using QuPath in 3 regions per section, and the number of pERK+ in the positive cells was counted to obtain the percentage of double positive cells.

Quantification of pERK and SOX9 fluorescent signal per cell. Two sections of day 7 post-fracture callus per sample were immunostained with both SOX9 and pERK antibodies. Three pictures were taken per section and cells or tdTom+ cells were manually delimited using ImageJ. SOX9 and pERK signal was quantified for each cell and values were plotted using GraphPad Prism to determine the correlation between SOX9 and pERK fluorescence.

RNAscope in situ hybridation

The expression of *Prss56* and *tdTom* at E12.5, 13.5 and 14.5 was visualized using the RNAscope® Multiplex Fluorescent Assay V2 (Biotechne). Embryos were dissected and the hindlimbs were fixed in ice-cold 4% PFA for 24 hours, before progressive sucrose incubation and cryoembedding. Expression of *Prss56*, *tdTom, Postn, Sox10, Osm, Pdgfa* and *Tgfb1* was assessed on adult tissue sections processed as described above. Twenty µm thick sections were cut and processed according to the manufacturer's protocol: 15 min of post-fixation in 4% PFA, ethanol dehydration, 10 min of H_2O_2 treatment, 5 min of target retrieval at 95°C, and 30 min of protease III treatment. After hybridization and revelation, the sections were mounted under a glass coverslip with Prolong Gold Antifade (P10144,

ThermoFischer). For adult sections, target retrieval and protease III treatment were replaced by an incubation in ACD custom reagent for 30 minutes at 40°C. Sections were pictured and analyzed using Zeiss LSM800 and the number of $tdTom^+$ and $Prss56^+$ cells per tibia per section was manually counted.

Primary periosteal cell culture

Mouse periosteal cell culture

Primary culture of murine periosteal cells was performed as previously described *(12, 59)*. Six- to 8-week-old mice were euthanized, and tibias were dissected free of muscle and surrounding tissue. Epiphyses were cut and bone marrow flushed. Flushed bones were placed in a culture-dish for explant culture with drops of culture medium composed of MEMα (32561094, ThermoFischer Scientific), supplemented with 20% of lot-selected Fetal Bovine Serum (10270106, ThermoFischer Scientific), 1% of Penicillin-Streptomycin and 10 ng/ml basic Fibroblast Growth Factor (bFGF, 3139-FB-025/CF, Biotechne). After cell migration, bone explants were removed. As previously reported, this protocol allows specific amplification of periosteal derived stem/progenitor cells, macrophages and osteoclasts *(13)*. Cells were trypsinized and used at passage 1 to 3. For in vivo cell transplantation of Prss56-derived cells, periosteal cells were cultured to passage 2, trypsinized and living tdTom+ were sorted using FACS Aria Fusion. Sorted tdTom+ cells were cultured one passage for cell amplification, trypsinized, counted and used for transplantation as described below.

Human periosteal cell culture

Primary culture of human periosteal cells was performed as described for murine periosteal cells. Periosteum collected at the pseudarthrosis site or the iliac crest was divided in several pieces and placed in a culture dish for explant culture with drops of culture medium composed of MEMα, supplemented with 20% of FBS, 1% of Penicillin-Streptomycin and 10 ng/ml bFGF. Drops of medium were replaced every day until the tissue attached to the culture dish. Periosteal cells progressively migrated in the dish. After 1 to 2 weeks, periosteum explants were removed and periosteal cells were trypsinized for further analyses. *NF1* genotyping and RNAseq analyses were performed at passage 1, in vivo transplantation at passage 2, in vitro proliferation, differentiation and MAPK pathway activation between passages 2 and 4.

Schwann cell and periosteal stem/progenitor cell transplantation

Schwann cell isolation

Prss56-derived Schwann cells were isolated from intercostal nerves *(60)*. Mice were euthanized and the back skin was incised. Nerves were collected free of surrounding tissues, minced and digested under constant agitation at 37°C in digestion buffer composed of Hanks Balanced Salt Solution (HBSS, 24020117, ThermoFischer Scientific) with 0,04% of Hyaluronidase (WOLS05474, Serlabo), 0,3% of Collagenase II, 0,15% of Trypsin and 100U/mL of DNAse I for 20 to 40 min. Digestion was stopped with MEMα medium supplemented with 20% of FBS. Cells were filtered, centrifuged, resuspended in MEMα with 20% FBS. Sytox Blue (S34857, Thermo Fisher Scientific) was added to stain dead cells and living $tdTom^+$ were sorted using Influx Cell Sorter.

Cell transplantation

Cell transplantation was performed as described in *(12, 51, 59)*. 100,000 cultured murine or human periosteal cells, isolated as described in the "Primary periosteal cell culture" section, or 3000 to 4000 tdTom+ Schwann cells were embedded in Tisseel Prima fibrin gel, composed of fibrinogen and thrombin (3400894252443, Baxter S.A.S, USA), according to manufacturer's instructions. Briefly, the cells were resuspended in 15 µL of fibrin (diluted at 1/4), before adding 15 µL of thrombin (diluted at 1/4) and mixing. The pellet was then placed on ice at least 15 min for polymerization. The cell pellet was transplanted at the fracture site.

In vitro proliferation

Cell proliferation was determined by cell counting every 2 days from day 2 to 10 after passage. 10,000 cells were plated in 24-well dish and cultured in culture medium only or supplemented with 1µM of selumetinib, SHP099, selumetinib and SHP099 or DMSO. The number of cells in each well was determined using the luminescent cell viability buffer CellTiter-Glo® (G7571, Promega, USA) according to the manufacturer's recommendation. Culture medium was removed and replaced by 0.7 ml of CellTiter-Glo® Buffer and 0.7 mL of fresh culture medium. After 30 min, the luminescence was measured using Tecan Infinite M200 Pro (Tecan, Switzerland). Each sample was analyzed in duplicates at each time point. Standard curve was used to determine the number of cells from absorbance values. Growth

curve was drawn and area under curve (AUC) was calculated using GraphPad Prism. AUC of periosteal cells from PA and IC was normalized on the AUC of the IC of each patient.

In vitro differentiation

In vitro differentiation was performed as described in *(59)*. For osteogenic and adipogenic differentiation, cells were plated and amplified in growth medium. At confluency, cells were cultured in osteogenic medium, containing MEMα with 10% lot selected FBS, 0.2mM L-ascorbic acid (A8960, Merck), 10mM glycerol 2- phosphate disodium salt hydrate (G9422, Merck) and 0.1 µM dexamethasone (D8893, Merck), or adipogenic medium, containing MEMα with 10% lot selected FBS, 10 µg/mL insulin (I3536, Merck), 100µM indomethacin (I7378, Merck), 0.5 mM 3-isobutyl-methylxanthine (I5879, Merck) and 0.1 µM dexamethasone (D8893, Merck). The medium was changed twice a week. After 21 days, cells were resuspended in Trizol (12034977, Thermo Fisher Scientific) and frozen for RNA analyses.

For chondrogenic differentiation, cells were plated as micromass of 5.10^5 cells in 200 µL of growth medium. After 4 hours, growth medium was replaced by chondrogenic medium containing high glucose DMEM with 10% FBS, 0.1 µM dexamethasone, 100 µg/mL sodium pyruvate (P5280, Merck), 40 µg/mL L-proline (P0380, Merck), 50 µg/mL L-ascorbic acid, 50 mg/mL Insulin-Transferrin-Selenium (I1884, Merck), and 10 ng/mL TGFβ1 (T7039, Merck). To test the impact of MEK-SHP2 inhibition treatment, the chondrogenic medium was supplemented with 1µM of selumetinib, SHP099, selumetinib and SHP099 or DMSO. After 3 days, micromasses were resuspended in Trizol and frozen for RNA analyses.

RNA extraction and qPCR

For qPCR analyses of *SOX9, RUNX2*, *COL1A1, ALPL* and *PPARG* from differentiated human pSSPCS, cells were collected in Trizol (15596026, Thermofisher) and RNAs were extracted following the manufacturer's instructions. After reverse transcription of 50ng to 1µg of RNA with Superscript II® (18064022, Thermofisher), cDNAs were amplified with Power SYBR Green System (4368706, Thermofischer) in 384 wells optical plates with the Roche LightCycler 480 Real-Time PCR System. Analyses were performed with the ΔΔCT method using *RPLP0* used as calibrator gene. The values of each sample were normalized on the iliac crest of the same patient. RT-qPCR were performed twice with duplicates for each data point. The primers sequences are listed in the Table S4.

To assess the expression of *Tgfb1* in *Prss56-Nf1* KO mice, the periosteum and hematoma from day 7 post-fracture callus were collected and snap frozen in liquid nitrogen. RNA was extracted using RNAeasy Plus Kit (74134, Qiagen) following manufacturer's instructions. RNA concentration was quantified using NanoDrop spectrophotometer (Thermo Scientific). Reverse transcription was performed using Superscript III RT® (18080-044, Life Technologies) following manufacturer's instructions. qPCR was performed by mixing 10 µL of SYBR green Master Mix, 5 µL of cDNA, 1 µL of primers and 4 µL of RNAse free H2O using StepOnePlus Real-Time PCR system (ThermoFischer). Analyses were performed with the ΔΔCT method using *Gapdh* as calibrator gene.

Western Blot

Cultured human periosteal cells were washed with 1X PBS and lysed on ice in RIPA buffer, 1X protease inhibitors (P8340, Merck) and 1X phosphatase inhibitors (4906845001, Merck). After 20 minutes of centrifugation at 17400 g and 4°C, protein concentrations were determined using the BCA protein assay kit (J63283.QA, ThermoFisher Scientific). Protein lysates (50µg) were migrated in SDS-polyacrylamide (Sodium Dodecyl Sulfate) 4-12% gel (Biorad) and transferred to nitrocellulose membranes (GE Healthcare). TBS-Tween was used for blocking solutions and to dilute the antibody solutions. Membranes were blocked for 1h with 5% BSA (Bovine Serum Albumin) and incubated at 4°C overnight with primary antibodies listed in the Table S3. Proteins were visualized using secondary antibodies conjugated to horseradish peroxidase. Images were obtained with the FusionFX imager (Vilbert) and chemiluminescence solutions (ECL, enhanced chemiluminescent, ThermoFisherScientific). Semi-quantitative analysis was done with ImageJ tools and signals were normalized on GAPDH signal. pERK signal on ERK signal was calculated for each sample, and each sample were normalized on the pERK/ERK signal of the IC of the same patient. To test the impact of MEK and SHP2 inhibition treatment on the activation of the MAPK pathway, PA pSSPCs were treated 4 hours with selumetinib, SHP099, selumetinib and SHP099 or DMSO at the indicated concentration before collection.

Bulk RNA sequencing of human primary periosteal cells

RNAs were extracted from primary periosteal cells from IC and PA site of patients 3 and 7 using the RNeasy Kit (Qiagen) and a DNA removal step according to manufacturer's recommendation. RNA qualities were assessed by capillary electrophoresis using High Sensitivity RNA reagents with the

Fragment Analyzer (Agilent Technologies) and the RNA concentrations were measured by using spectrophometry using Xpose (Trinean) and Fragment Analyzer capillary electrophoresis. RNAseq libraries were prepared from 1 µg of total RNA using the Universal Plus mRNA-Seq kit (Nugen) as recommended by the manufacturer. The oriented cDNAs produced from the poly-A+ fraction were sequenced on a NovaSeq6000 from Illumina (Paired-End reads 100 bases + 100 bases). A total of ~22 millions of passing filter paired-end reads was produced per library. FASTQ files were mapped to the ENSEMBL Human (GRCh38/hg38) reference using HISAT2 and counted by featureCounts from the Subread R package. Read count normalization and group comparisons were performed by three independent and complementary statistical methods: Deseq2, edgeR, LimmaVoom. Flags were computed from counts normalized to the mean coverage. All normalized counts <20 were considered as background. The results of the three methods were filtered at pvalue<0.05 and folds 1.2 compared and grouped by Venn diagram. Principal component analysis was performed using Rstudio v1.4.1717 and Gene Ontology analyses using EnrichR (maayanlab.cloud/Enrichr/).

Flow Cytometry analyses of periosteal, bone marrow and skeletal muscle cells

Periosteal cell isolation

To isolate periosteal cells, uninjured tibia were collected from *Prss56-Nf1*$^{+/+}$ and *Prss56-Nf1*$^{fl/fl}$ mice, by carefully removing all surrounding soft tissues *(61)*. Epiphyses were embedded in low melting agarose and tibias were placed for 30 min at 37°C in digestion medium composed of PBS with 3mg/ml of Collagenase B (C6885, Merck), 4mg/ml of Dispase (D4693, Merck) and 100U/mL of DNAse I (WOLS02007, Serlabo, France). After digestion, tibias were removed and the suspension was filtered, centrifuged, and resuspend in the appropriate buffer for subsequent analyses.

Bone marrow cell isolation

The bone marrow was flushed using MEMα with 10% FBS. The flushed bone marrow was centrifuged and resuspend in ACK buffer (A1049201, Thermo Fisher Scientific) for red blood cells lysis for 5 min at room temperature. After centrifugation, the bone marrow was resuspended in digestion medium composed of PBS with 3mg/ml of Collagenase B, 4mg/ml of Dispase and 100U/mL of DNAse I and placed at 37°C for 30 min. After digestion, the suspension was filtered, centrifuged and resuspended in PBS with 0,5% BSA and 2mM EDTA (EU00084, Euromedex). A step of hematopoietic cell depletion was performed to increase the mesenchymal fraction of the cell suspension using lineage cell depletion

kit following the manufacturer's instructions. Bone marrow cells were incubated with primary biotinylated antibodies specific to hematopoietic lineage (CD5, CD45R (B220), CD11b, Gr-1 (Ly-6G/C), 7-4, and Ter-119) followed by an incubation with Anti-Biotin microbeads and magnetic column filtering (130-090-858, Milteny Biotec, Germany). After depletion, cells were centrifuged and resuspended in the appropriate buffer for subsequent analyses.

Skeletal muscle mononucleated cell isolation

Skeletal muscle mononucleated cells were isolated as described *(51)*. The skeletal muscles surrounding the tibia were dissected free of fascia, tendon and fat. Tissues were minced and digested at 37°C for 2 hours in DMEM (21063029, Life Technologies) with 1% Trypsin (15090046, Life Technologies) and 1% collagenase D (11088866001, Roche). Cells in suspension were removed every 20 min and digestion medium was replaced. After 2 hours, the cell suspension was filtered, centrifuged, and resuspended in the appropriate buffer for subsequent analyses.

Flow cytometry analyses

For flow cytometry analyses of digested tissues, cell suspensions were prepared as described above. For cultured cells, cells were trypsinized, centrifuged and resuspended in FACS buffer, composed of PBS with 0,5% BSA and 2mM EDTA. Cells were incubated with antibodies listed in Table S3 for 30 min, on ice and protected from light. After washing, cells were resuspended in FACS buffer and Sytox Blue (S34857, Thermo Fisher Scientific) was added before analysis to stain dead cells. Analyses were performed using a BD Fortessa X20 (BD Biosciences). Compensation matrix was designed using Compensation Beads (01-2222-42, Thermo Fischer Scientific) and appropriate controls were used to delimitate the gating strategy. Data were analyzed using FlowJo v10.8.1.

Nuclei extraction for single nuclei RNAseq

Nuclei extraction from murine periosteum

Five datasets were used for this study: (i) uninjured periosteum from wild-type mice, (ii) periosteum and hematoma 3 days post-fracture from wild-type mice, (iii) periosteum and hematoma 5 days post-fracture from wild-type mice, (iv) periosteum and hematoma 7 days post-fracture from control mice and (v) periosteum and hematoma 7 days post-fracture from *Prss56-Nf1*$^{fl/fl}$ mice. Datasets (i), (ii),(iii) and (iv) were from *(16)* and dataset (v) was generated for this study. All samples were generated using the following protocol. Nuclei extraction protocol was adapted from *(62, 63)*. For uninjured periosteum, tibias from 4 mice were dissected free of muscle and surrounding tissues. The epiphyses were cut, and the bone marrow flushed. The periosteum was scraped from the cortex using Dissecting Chisel (10095-12, Fine Science Tools). For days 3, 5 and 7 post-fracture, injured tibias from 4 to 9 mice were collected and the surrounded tissues were removed. The activated periosteum was scraped and collected with the hematoma. Collected tissues were minced and placed 5 min in ice-cold Nuclei Buffer (NUC101, Merck) before mechanical nuclei extraction using a glass douncer. Extraction was performed by 20 strokes of pestle A followed by 10-20 of pestle B. Nuclei suspension was filtered, centrifuged, and resuspended in RNAse-free PBS (AM9624, ThermoFischer Scientific) with 2% Bovine Serum Albumin (A2153, Merck) and 0.2 U/µL RNAse inhibitor (3335399001, Roche). A second step of centrifugation was performed to reduce contamination by cytoplasmic RNAs. Sytox™ AADvanced™ (S10349, ThermoFischer Scientific) was added (1/200) to label nuclei and Sytox-AAD+ nuclei were sorted using Sony SH800.

Nuclei extraction from human periosteum

Nuclei extraction was performed on snap-frozen human periosteum samples from PA site of patients P5 and P13 and from IC of patients P5 and P15. RNA integrity was checked beforehand on identical tissue samples (RIN > 6.5). Periosteum samples were briefly defrosted in nuclei extraction buffer before mincing and nuclei extraction as described above for murine periosteum. Gating strategy is reported in Figure S9B.

Single nuclei RNA sequencing

The snRNA-seq libraries were generated using Chromium Single Cell Next GEM 3′ Library & Gel Bead Kit v.3.1 (10x Genomics) according to the manufacturer's protocol. Briefly, 10 000 to 20 000 nuclei were loaded in the 10x Chromium Controller to generate single-nuclei gel-beads in emulsion. After reverse transcription, gel-beads were disrupted. Barcoded complementary DNA was isolated and amplified by PCR. Following fragmentation, end repair and A-tailing, sample indexes were added during index PCR. The purified libraries were sequenced on a Novaseq (Illumina) with 28 cycles of read 1, 8 cycles of i7 index and 91 cycles of read 2. Sequencing data were processed using the Cell Ranger Count pipeline and reads were mapped on the mm10 reference mouse genome or HG38 2020-A reference human genome, with intronic and exonic sequences.

Single nuclei RNA sequencing analyses

Single-nuclei RNAseq analyses were performed using Seurat v4.1.0 *(64, 65)* and Rstudio v1.4.1717.

Filtering and clustering

Aligned snRNAseq datasets were filtered to retain only nuclei expressing between 200 and 5000 genes and expressing less than 0,5% of mitochondrial genes and 2.5% of ribosomal genes. Contamination from myogenic cells was removed from the analyses. After filtering, the datasets of murine samples were composed of 471 and 722 cells for uninjured datasets, 1634 nuclei from day 3 post-fracture datasets, 2114 nuclei for day 5 post-fracture dataset, 1058 nuclei for control day 7 post-fracture dataset and 1113 nuclei for *Prss56-Nf1*$^{fl/fl}$ day 7 post-fracture dataset.

Uninjured, d3, d5 and control d7 datasets were integrated using Seurat and Harmony *(66)*. The datasets were merged and scaled on mitochondrial and ribosomal content. Clustering was performed using the first 20 principal components and a resolution of 2. SSPC, fibrogenic, chondrogenic and osteogenic clusters from the integration were isolated to perform subset analyses. The subset was reclustered using the first 20 principal components and a resolution of 0.5.

Day 7 post-fracture datasets from control and *Prss56-Nf1*$^{fl/fl}$ mice were integrated. The integrated dataset was regressed on mitochondrial and ribosomal content. Clustering was performed using the first 35 principal components and a resolution of 0.8. SSPC, fibrogenic, chondrogenic and osteogenic clusters from the integration were isolated to perform subset analyses. The subset was reclustered using

the first 25 principal components and a resolution of 1. Gene ontology analyses were performed using EnrichR.

Human periosteum samples were filtered to retain only nuclei expressing between 200 and 5000 genes and expressing less than 2% of mitochondrial genes and 2.5% of ribosomal genes. Contamination from myogenic cells was removed from the analyses. After filtering, the datasets of human samples were composed of 395 nuclei for the PA periosteum of P5, 1996 cells for the IC periosteum of P15, 1216 nuclei for the IC periosteum of P13, and 8011 nuclei for the PA periosteum of P13. To allow comparison between datasets, the number of nuclei in the dataset of PA periosteum of P13 was reduced to 2250 nuclei using random selection. Datasets were integrated with regression on mitochondrial and ribosomal content and clustering using the first 10 principal components and a resolution of 0.8.

Pseudotime analysis

Monocle3 v1.0.0 was used for pseudotime analysis *(67)*. Single-cell trajectories were determined using monocle3 default parameters. The starting point of the pseudotime trajectory was determined as the cells from the uninjured dataset with the highest expression of stem/progenitor marker genes *(Ly6a, Cd34, Dpp4, Pi16)*.

Lineage and MAPK score

Lineage score was calculated by the mean of the expression of specific markers listed in Table S5 for murine samples and Table S6 for human samples. For cell type identification, common markers from the literature were used. To assess the activation of the MAPK pathway and the cellular response to TGFβ, the list of genes from the Gene Ontology “positive regulation of MAPK cascade” and “Cellular response to TGFβ stimulus” were used respectively. To compare the cellular response to TGFβ of the different clusters between control and *Prss56-Nf1*$^{fl/fl}$ datasets, the average lineage score per cluster per dataset was calculated, and the lineage score in *Prss56-Nf1*$^{fl/fl}$ dataset was normalized on the lineage score of control dataset.

Analyses of published datasets from Kelly *et al.*

To assess the expression of Prss56 in developing limb, we analyzed a single cell-RNAseq dataset from *(68)* (GSE142425). Murine limbs from E11.5, E13.5, E15.5 and E18.5 embryos were digested and living

cells were processed for single cell RNA-sequencing using the 10X genomics platform. A total of 9939 cells were obtained. The provided data were reanalyzed and clustered using UMAP projection.

Supplementary Figures

Figure S1

A

Patients with tibia and fibula PA

#Patient	1st hit	Blood	2nd hit tibia	2nd hit fibula
P4	c.3721C>T	*NF1+/-*	cnLOH	possible cnLOH#
P5	c.1722-?_1842+?del	*NF1+/-*	c.6619C>T	c.6619C>T
P9	c.2752A>T	WT	cnLOH	Not identified
P11	Not identified	WT	cnLOH	cnLOH
P13	c.1722-2 IVS15	*NF1+/-*	cnLOH	cnLOH

B

#Patient	Blood	1st hit	2nd hit periosteum	2nd hit muscle	2nd hit skin
P3	WT	c.5599delA	c.2033dupC	c.2033dupC	c.2033dupC
P7	WT	c.1797G>A	c.1570G>T	c.1570G>T	c.1570G>T
P15	WT	c.5839C>T	c.574C>T	c.574C>T	-

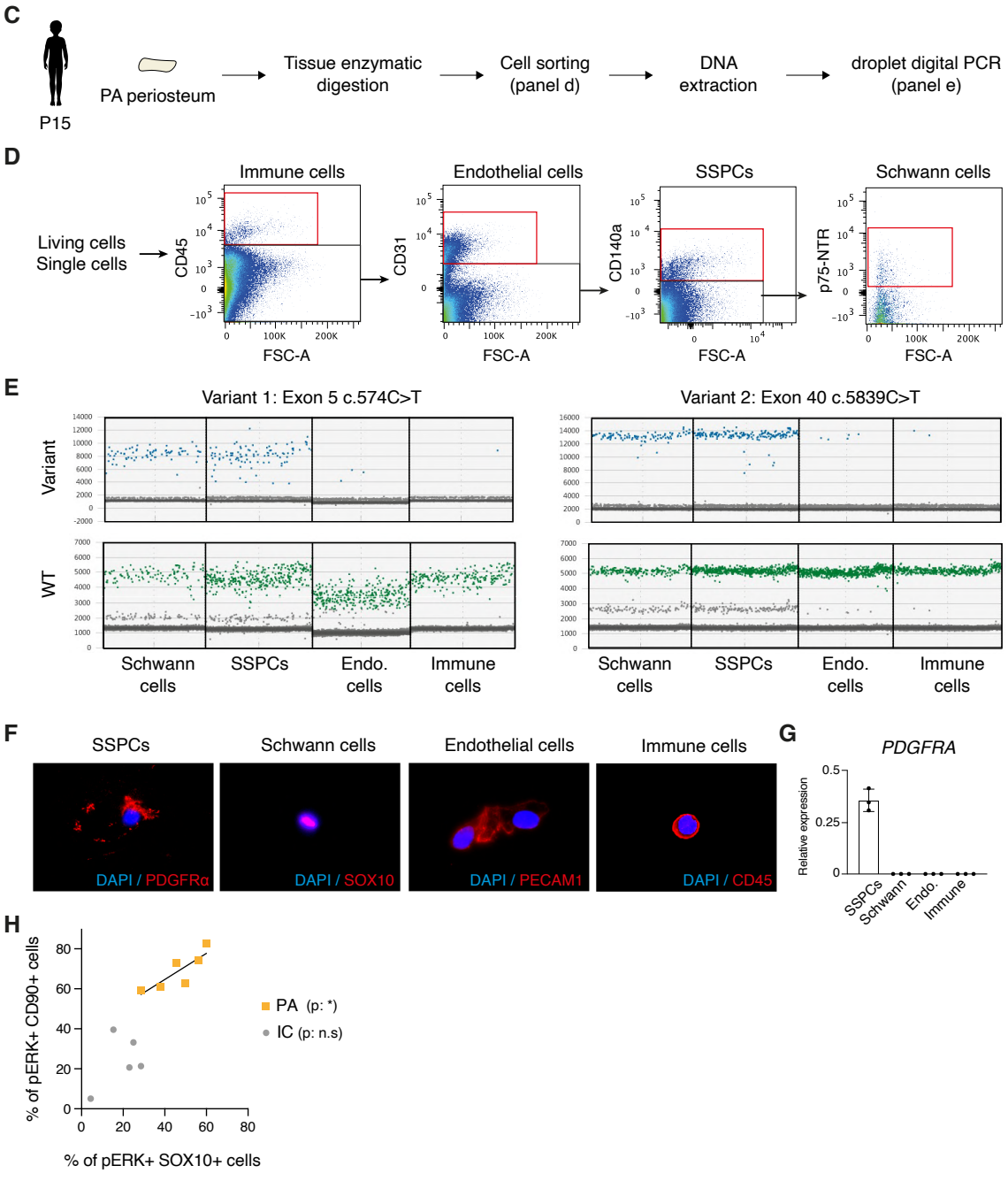

Figure S1: Genetic analyses of human pathological periosteum

A. *NF1* sequencing of 5 patients with combined tibia and fibula pseudarthrosis. The presence of the same second *NF1* hit in the tibia and fibula PA is detected in 4/5 patients. #Imbalance in informative SNP rs146315101 suggests a cnLOH. **B.** *NF1* sequencing shows the presence of the same 2nd *NF1* hit in the periosteum, muscle and skin at the PA site in patients P3 and P7, and in periosteum and muscle in patient P15. **C.** Experimental design. PA periosteum from patient P15 was enzymatically digested and the different cell populations sorted, before DNA extraction and droplet digital PCR (ddPCR) or immunofluorescence. **D.** Gating strategy used to sort immune cells, endothelial cells, Schwann cells and SSPCs from the digested periosteum of patient P15. **E.** Fluorescence intensity of the droplets after amplification of variant 1 (c.574C>T, left) and variant 2 (c.5839C>T, right) using the ddPCR assay. Detection of the variant allele is in blue (top panels) and detection of the wild-type allele in green (bottom panels). The variant allele is detected only in Schwann cells and SSPCs for both variants. **F.** Immunofluorescence for PDGFRα, SOX10, PECAM1 and CD45 on sorted SSPCs, Schwann cells, endothelial cells, and immune cells respectively. **G.** Relative expression of *PDGFRA* detected in sorted SSPCs, but not in Schwann cells, endothelial cells and immune cells, indicating the absence of SSPCs in the other cell populations. **H.** Correlation between the percentage of pERK+ pSSPCs and Schwann cells in the human periosteum from the pseudarthrosis site (orange) and iliac crest (grey). Pearson's correlation test showed correlation in PA tissues (p-value: 0.04, r=0.83) but not with IC tissues (p-value: 0.36, r=0.52). #Absence of SNP imbalance shows the absence of cnLOH in the fibrous tissue. WT: wild-type, cnLOH: copy neutral loss of heterozygosity. VAF: variant allele frequency. Endo: endothelial.

Figure S2

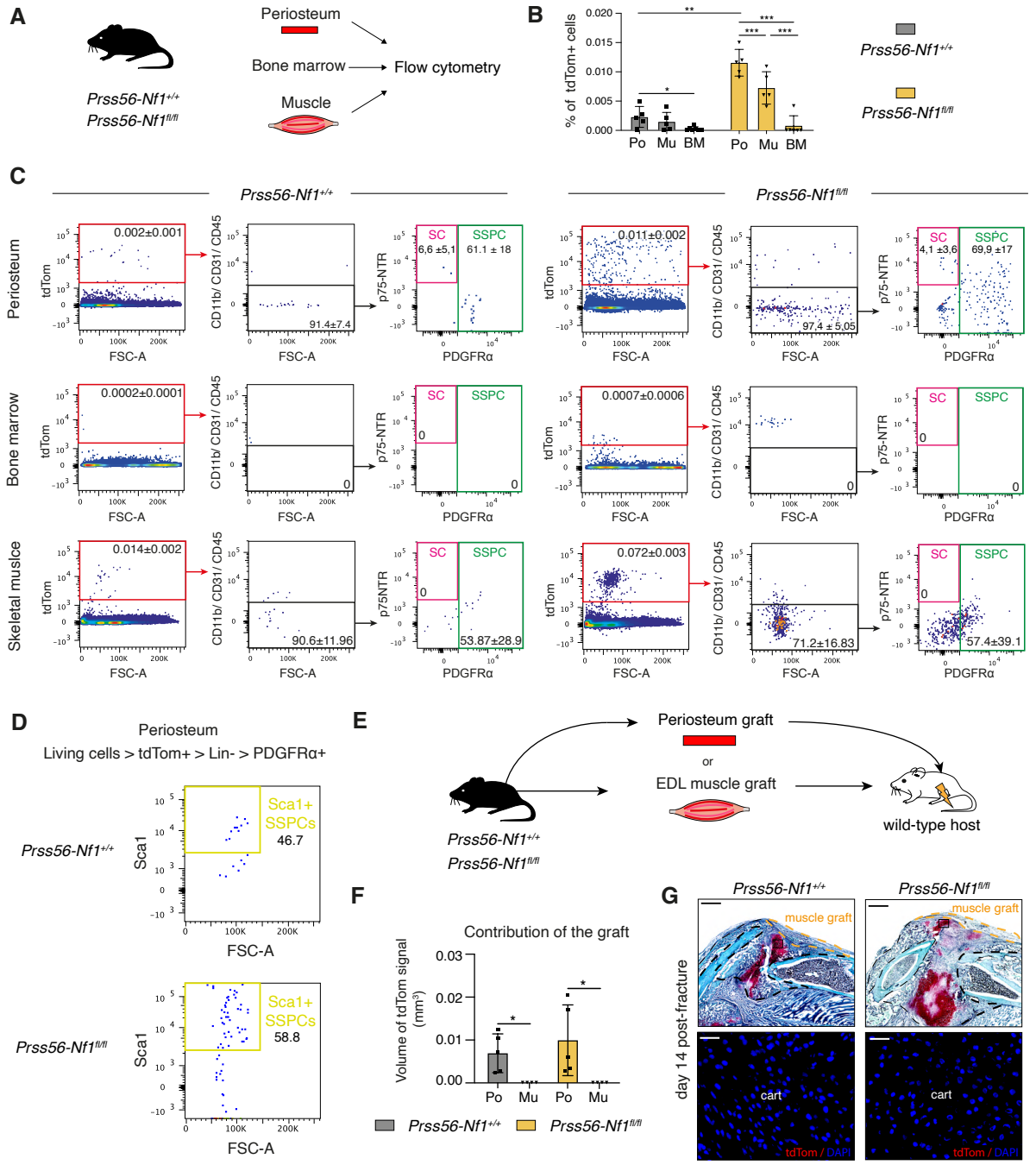

Figure S2: Periosteum is the only source of BC-derived cells contributing to callus fibrosis in *Prss56-Nf1* KO mice

A. Experimental design. Periosteum, bone marrow, and skeletal muscle (i.e. the three sources of SSPCs for bone repair) were collected from *Prss56-Nf1*$^{+/+}$and *Prss56-Nf1*$^{fl/fl}$ mice and digested for flow cytometry analyses. **B.** Percentage of tdTom+ cells in periosteum (Po), skeletal muscle (Mu) and bone marrow (BM) of *Prss56-Nf1*$^{+/+}$and *Prss56-Nf1*$^{fl/fl}$ mice (n=5-7 mice per group). **C.** Flow cytometry analyses of

tdTom+ cells isolated from periosteum, bone marrow and skeletal muscle of *Prss56-Nf1*$^{+/+}$and *Prss56-Nf1*$^{fl/fl}$ mice showing the presence of tdTom+ Lin- (CD11b-, CD31-, CD45-) PDGFRα+ SSPCs in the periosteum and skeletal muscle and tdTom+ Lin- p75-NTR+ Schwann cells (SC) in the periosteum but absence of tdTom+ Lin- cells in bone marrow. (n=5-7 mice per group). **D.** Flow cytometry analyses of tdTom+ pSSPCs from *Prss56-Nf1*$^{+/+}$ and *Prss56-Nf1*$^{fl/fl}$ mice showing that around 50% of PDGFRα+ cells are positive for the stemness marker SCA1. **E.** Experimental design. EDL muscles or periosteum were collected from *Prss56-Nf1*$^{+/+}$and *Prss56-Nf1*$^{fl/fl}$ mice and grafted at the fracture site of a wild-type host. **F.** Volume of tdTom signal in the callus of wild-type host at 14 days post-fracture and periosteum (Po) or skeletal muscle (Mu) graft isolated from *Prss56-Nf1*$^{+/+}$or *Prss56-Nf1*$^{fl/fl}$ mice. Only tdTom+ cells recruited from the periosteum contribute to the callus. (n= 4-6 mice per group) **G.** Representative Safranin'O (SO) staining of callus section at day 14 post-fracture and EDL muscle graft from *Prss56-Nf1*$^{+/+}$or *Prss56-Nf1*$^{fl/fl}$ mice (graft delimited by the orange dashed line). High magnification of the cartilage in adjacent sections showing the absence of contribution of Prss56-derived cells from the skeletal muscle of *Prss56-Nf1*$^{+/+}$and *Prss56-Nf1*$^{fl/fl}$ mice to the host callus. Cart: cartilage. * $p < 0.05$, *** $p < 0.001$. Scale bars: Low magnification: 1mm. High magnification: 50 µm.

Figure S3

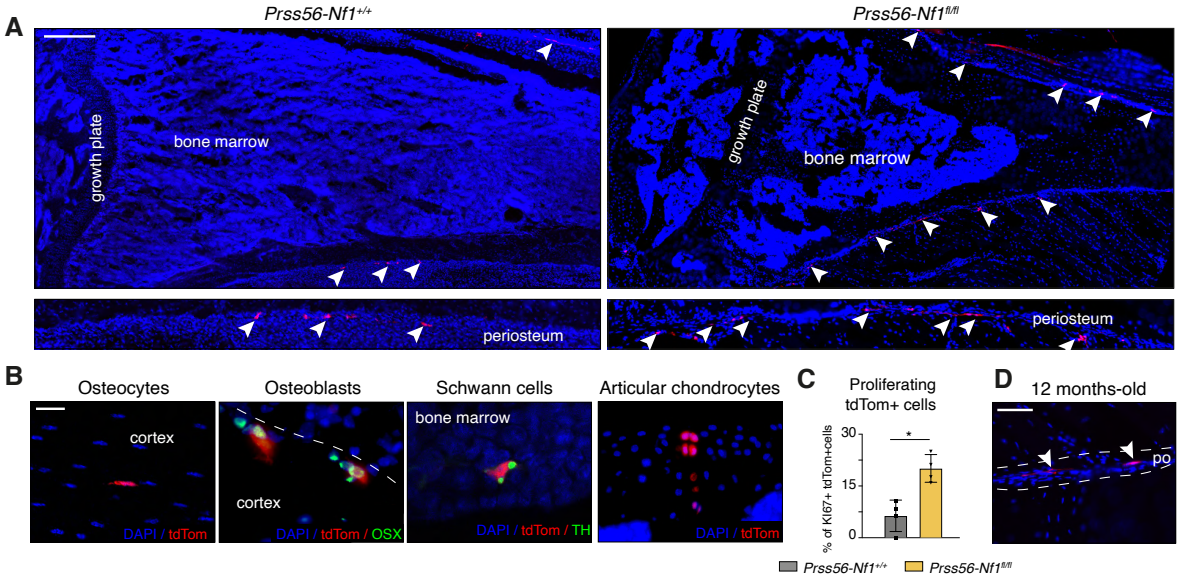

Figure S3: Lineage tracing of Prss56-derived cells in uninjured tibia

A. Tibial section of 3 months-old tibia from *Prss56-Nf1*$^{+/+}$ and *Prss56-Nf1*$^{+/+}$ mice showing the presence of tdTom+ cells in the periosteum (white arrows). **B.** Lineage tracing showing the presence of tdTom+ osteocytes, osteoblasts, bone marrow Schwann cells and articular chondrocytes in the tibia from *Prss56-Nf1*$^{+/+}$ mice. **C.** Percentage of proliferating tdTom+ cells in the periosteum of 3 months-old *Prss56-Nf1*$^{+/+}$ mice (n=4 per group). **D.** Lineage tracing showing the presence of tdTom+ cells in the tibia of 12 months-old *Prss56-Nf1*$^{+/+}$ mice. Scale bar. A. 200 µm B: 20 µm. D: 125 µm. * $p < 0.05$

Figure S4

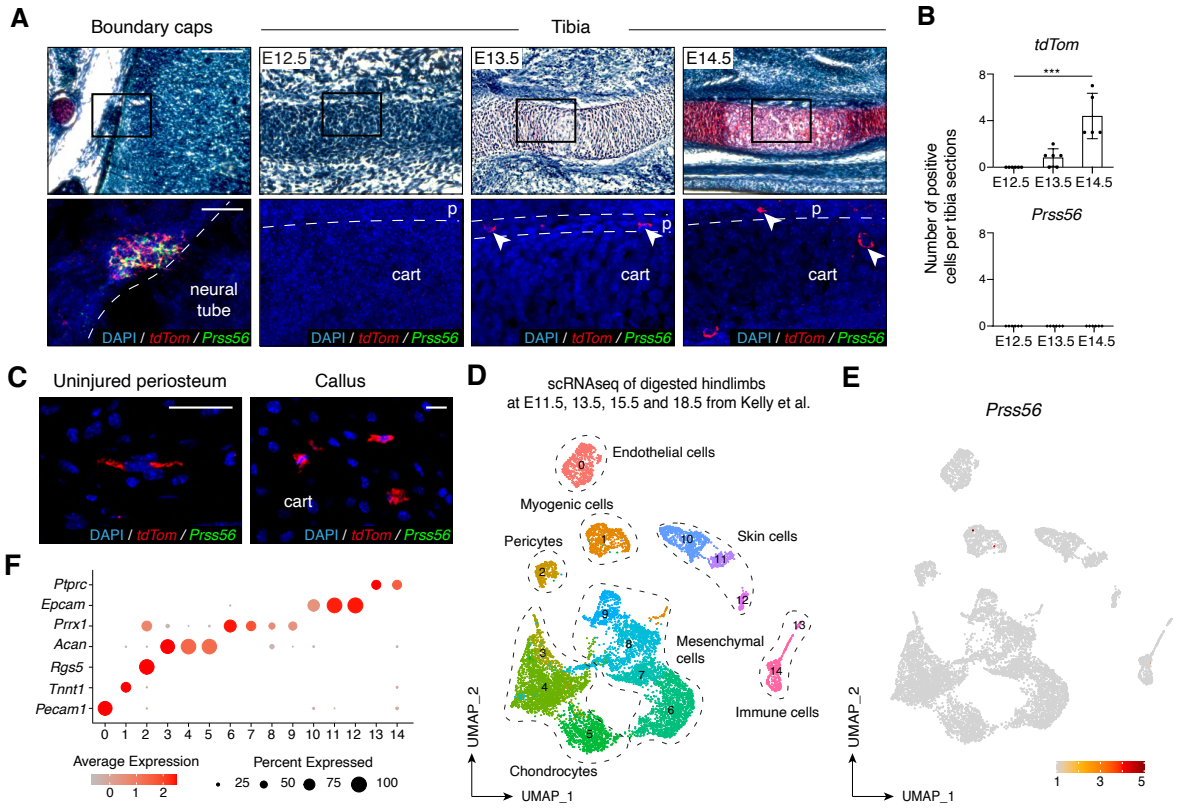

Figure S4: *Prss56* expression in boundary cap (BC) and localization of BC derivatives in tibia during bone development

A. Safranin'O staining and RNAscope experiments using *tdTom* and *Prss56* probes on boundary cap (BC) and tibia sections from E12.5, E13.5 and E14.5 *Prss56-Nf1*$^{+/+}$ embryos showing that *Prss56* expression is restricted to the BC and is not detected in BC-derived cells within developing tibia. TdTom+ cells are detected within the perichondrium (p) from E13.5 and the cartilaginous matrix (cart) from E14.5 (white arrowheads). **B.** Number of *tdTom* and *Prss56* expressing cells per tibia sections of E12.5, E13.5 and E14.5 *Prss56-Nf1*$^{+/+}$ embryos showing the increased number of BC derivatives in tibia during bone development (n=5-6 embryos per group). **C.** RNAscope experiments using *tdTom* and *Prss56* probes on uninjured periosteum and day 7 post-fracture callus of 3-month-old *Prss56-Nf1*$^{+/+}$ mice showing no expression of *Prss56* in *tdTom* expressing cells and confirming the presence of BC derivatives in adult tibial periosteum. **D.** UMAP projection of integrated scRNAseq datasets from digested hindlimbs at E11.5, E13.5, E15.5 and E18.5 from *(16)*. **E.** Feature plot of *Prss56* gene expression showing absence of *Prss56* expression in mesenchymal clusters at these embryonic stages. **f.** Dot plot of genes identifying endothelial cells (*Pecam1*), myogenic cells (*Tnnt1*), pericytes (*Rgs5*), chondrogenic cells (*Acan*),

mesenchymal cells (*Prrx1*), skin cells (*Epcam*), and immune cells (*Ptprc*). Cart: cartilage. Scale bars: Panel A: 75 μm, Panel C: 25μm.

Figure S5

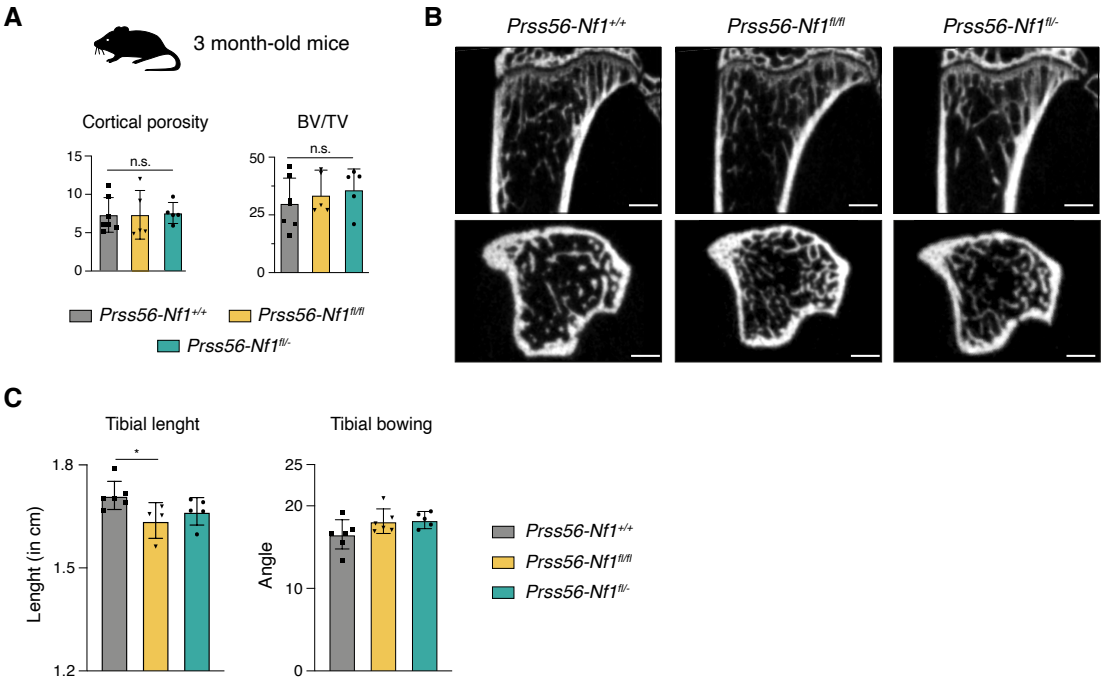

Figure S5: Bone phenotype of *Prss56-Nf1* KO mice

A. Cortical porosity and bone volume/total volume (BV/TV) of trabecular bone of uninjured tibia from 3-month-old *Prss56-Nf1*$^{+/+}$, *Prss56-Nf1*$^{fl/fl}$ and *Prss56-Nf1*$^{fl/-}$ mice (n = 5-7 mice per group). **B.** Representative longitudinal and transverse microCT images of uninjured tibia from 3-month-old *Prss56-Nf1*$^{+/+}$, *Prss56-Nf1*$^{fl/fl}$ and *Prss56-Nf1*$^{fl/-}$ mice. **C.** Tibial length and curvature of uninjured tibia from 3-month-old *Prss56-Nf1*$^{+/+}$, *Prss56-Nf1*$^{fl/fl}$ and *Prss56-Nf1*$^{fl/-}$ mice (n = 5-6 mice per group). p-value: * $p < 0.05$, n.s.: non-significant. Scale bar: 500µm.

Figure S6

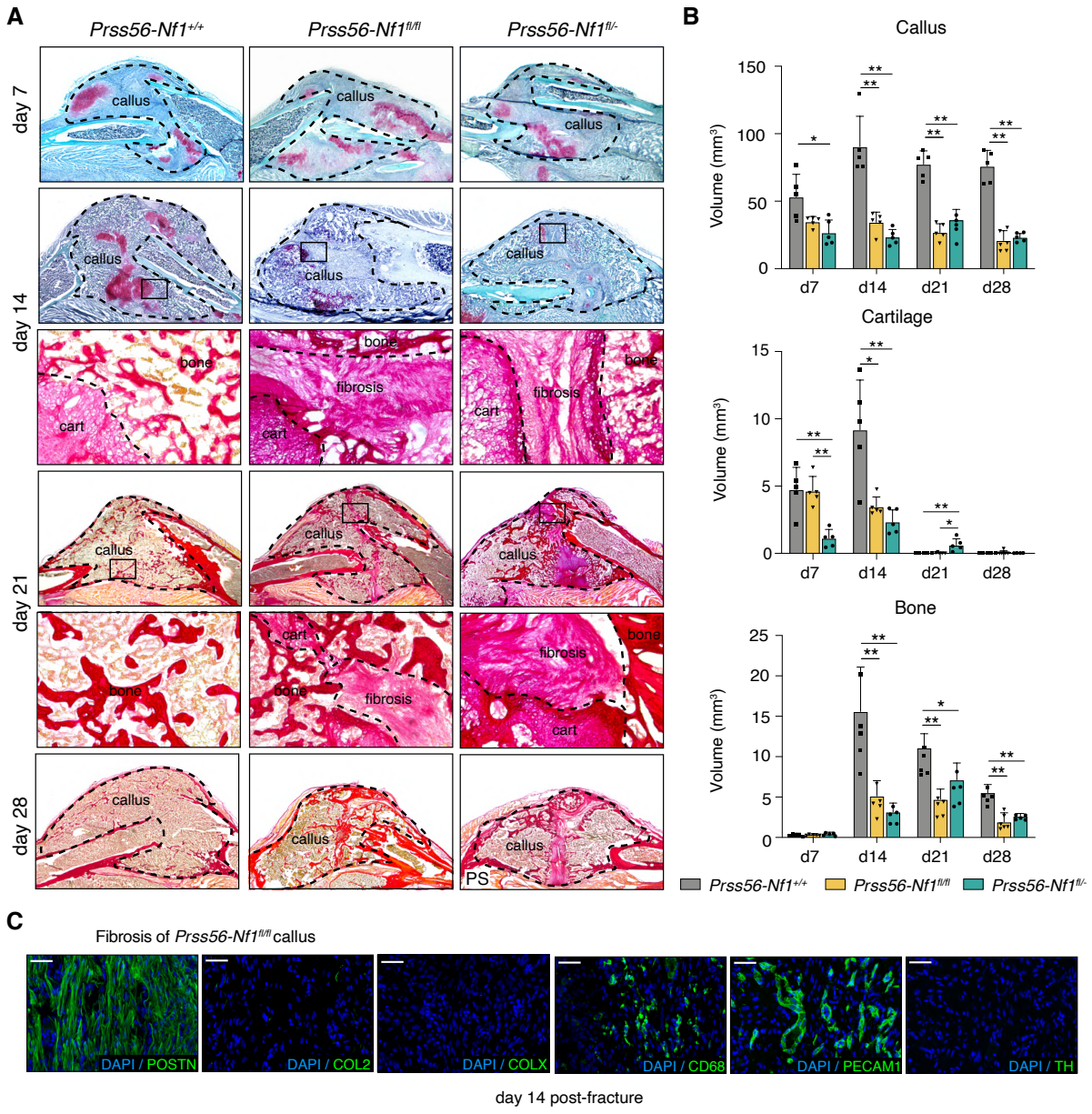

Figure S6: Fracture nonunion in *Prss56-Nf1 KO* mice

A. Representative callus sections of *Prss56-Nf1*$^{+/+}$, *Prss56-Nf1*$^{fl/fl}$ and *Prss56-Nf1*$^{fl/-}$ mice at 7, 14, 21 and 28 days post tibial fracture stained with Safranin'O (SO) and Picrosirius (PS) and high magnification images showing the persistent fibrosis accumulation in *Prss56-Nf1*$^{fl/fl}$ and *Prss56-Nf1*$^{fl/-}$ mice. **B.** Histomorphometric quantification of the volume of callus, cartilage, and bone at days 7, 14, 21 and 28 post-fracture in *Prss56-Nf1*$^{+/+}$, *Prss56-Nf1*$^{fl/fl}$ and *Prss56-Nf1*$^{fl/-}$ mice. (n=5-6 mice per group). **C.** Immunofluorescence on fibrotic callus tissue at day 28 post-fracture in *Prss56-Nf1*$^{fl/fl}$ mice showing expression of the extracellular matrix protein periostin (POSTN), but not Collagen II (COL2), Collagen

X (COLX), and expression of the immune marker CD68 and the endothelial marker PECAM1 but no expression of the nerve marker TH (n=3 sections from 3 mice). p-value: * $p < 0.05$, ** $p < 0.01$. Scale bar: Panel A :500µm, Panel C: 100µm.

Figure S7

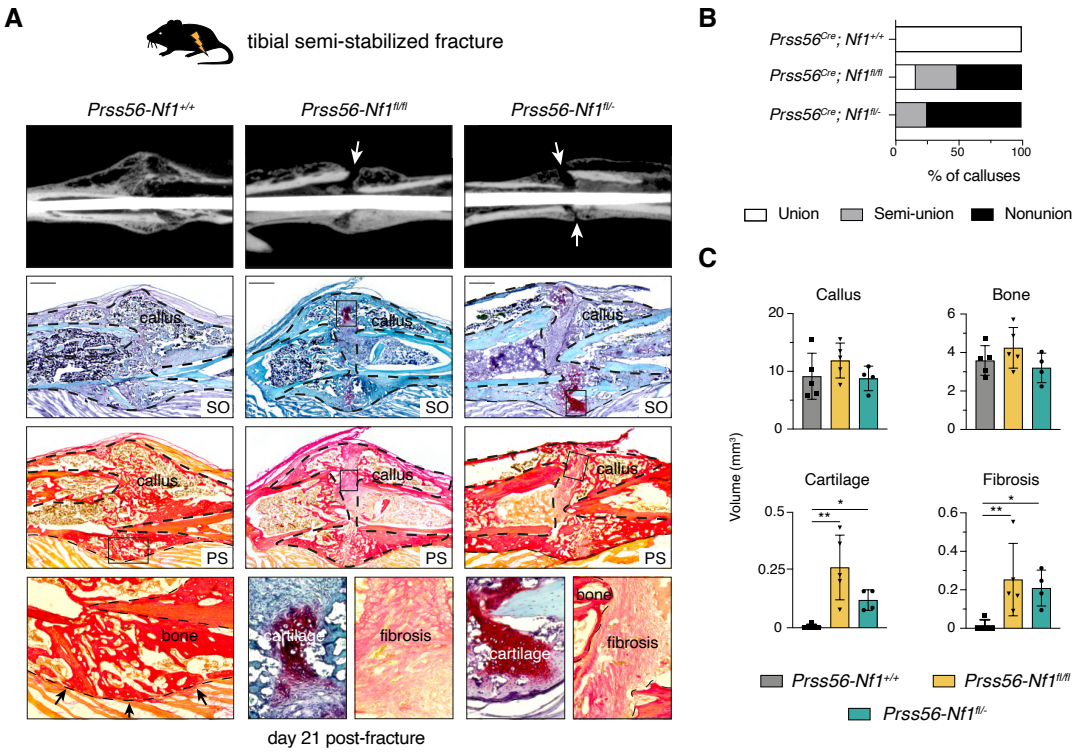

Figure S7: *Prss56-Nf1 KO* mice exhibit fracture nonunion in a semi-stabilized fracture model

A. Top: Representative microCT images of callus from *Prss56-Nf1*$^{+/+}$, *Prss56-Nf1*$^{fl/fl}$ and *Prss56-Nf1*$^{fl/-}$ mice at 21 days post-fracture, showing absence of bone bridging in *Prss56-Nf1*$^{fl/fl}$ and *Prss56-Nf1*$^{fl/-}$ mutant mice (white arrows). Bottom: Representative callus sections of *Prss56-Nf1*$^{+/+}$, *Prss56-Nf1*$^{fl/fl}$ and *Prss56-Nf1*$^{fl/-}$ mice at 21 days post semi-stabilized fracture stained with Safranin'O (SO) and Picrosirius (PS) and high magnification images showing unresorbed cartilage and persistent fibrosis accumulation in *Prss56-Nf1*$^{fl/fl}$ and *Prss56-Nf1*$^{fl/-}$ mice. **B.** Percentage of calluses from *Prss56-Nf1*$^{+/+}$, *Prss56-Nf1*$^{fl/fl}$ and *Prss56-Nf1*$^{fl/-}$ mice showing bone union (white), semi-union (grey) or nonunion (black) on microCT scan 21 post-fracture (n=4-5 mice per group). **C.** Histomorphometric quantification of the volume of callus, cartilage, bone and fibrosis at days 21 post-fracture of *Prss56-Nf1*$^{+/+}$, *Prss56-Nf1*$^{fl/fl}$ and *Prss56-Nf1*$^{fl/-}$ mice. (n=4-5 mice per group). p-value: * $p < 0.05$, ** $p < 0.01$.

Figure S8

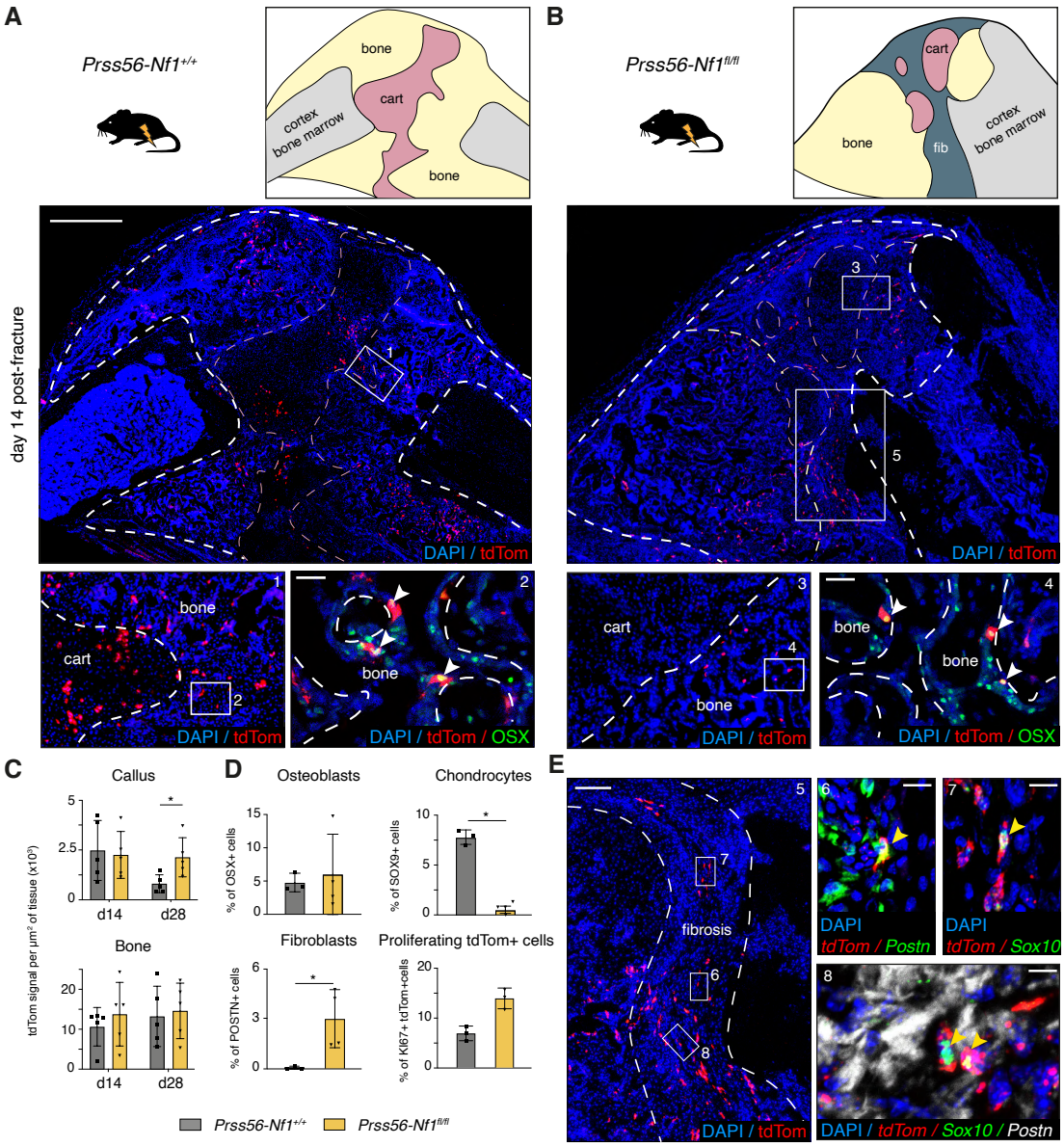

Figure S8: Spatial distribution of BC-derived cells in the fracture callus

A. (top) Callus section of day 14-post fracture callus of *Prss56-Nf1*$^{+/+}$ mice and schematic representation of the bone (yellow) and cartilage (pink). (bottom) High magnification of the cartilage-bone transition zone showing the presence of tdTom+ cells in cartilage and bone (1) and immunofluorescence showing that tdTom+ cells in bone are OSX+ osteoblasts (2). **B.** (top) Callus section of day 14-post fracture callus of *Prss56-Nf1*$^{fl/fl}$ mice and schematic representation of the bone (yellow), cartilage (pink) and fibrosis (green). (bottom) High magnification of the cartilage-bone transition zone showing the presence of tdTom+ cells only in bone (3) and immunofluorescence showing that tdTom+ cells in bone are OSX+

osteoblasts. (4) **C.** Quantification of tdTom+ signal in callus and bone of *Prss56-Nf1*$^{+/+}$ and *Prss56-Nf1*$^{fl/fl}$ mice 14- and 28-days post-fracture (n=5 mice per group). **D.** Percentage of tdTom+ OSX+ osteoblasts, SOX9+ chondrocytes, POSTN+ fibroblasts, and Ki67+ proliferating cells in the day 14-post fracture callus of *Prss56-Nf1*$^{+/+}$ and *Prss56-Nf1*$^{fl/fl}$ mice (n=3-4 per group). **E.** High magnification of the fibrosis tissue in the callus of *Prss56-Nf1*$^{fl/fl}$ mice (5) and RNAscope experiments to show the distribution of *tdTom* and *Postn*-expressing fibroblasts (6), tdTom-*Sox10*-expressing Schwann cells (7) and Schwann cells surrounding by WT-fibroblasts (8). p-value: * $p < 0.05$. Scale bar: Panel A: 1mm, Panel E: low magnification: 250µm, high magnification: 50µm.

Figure S9

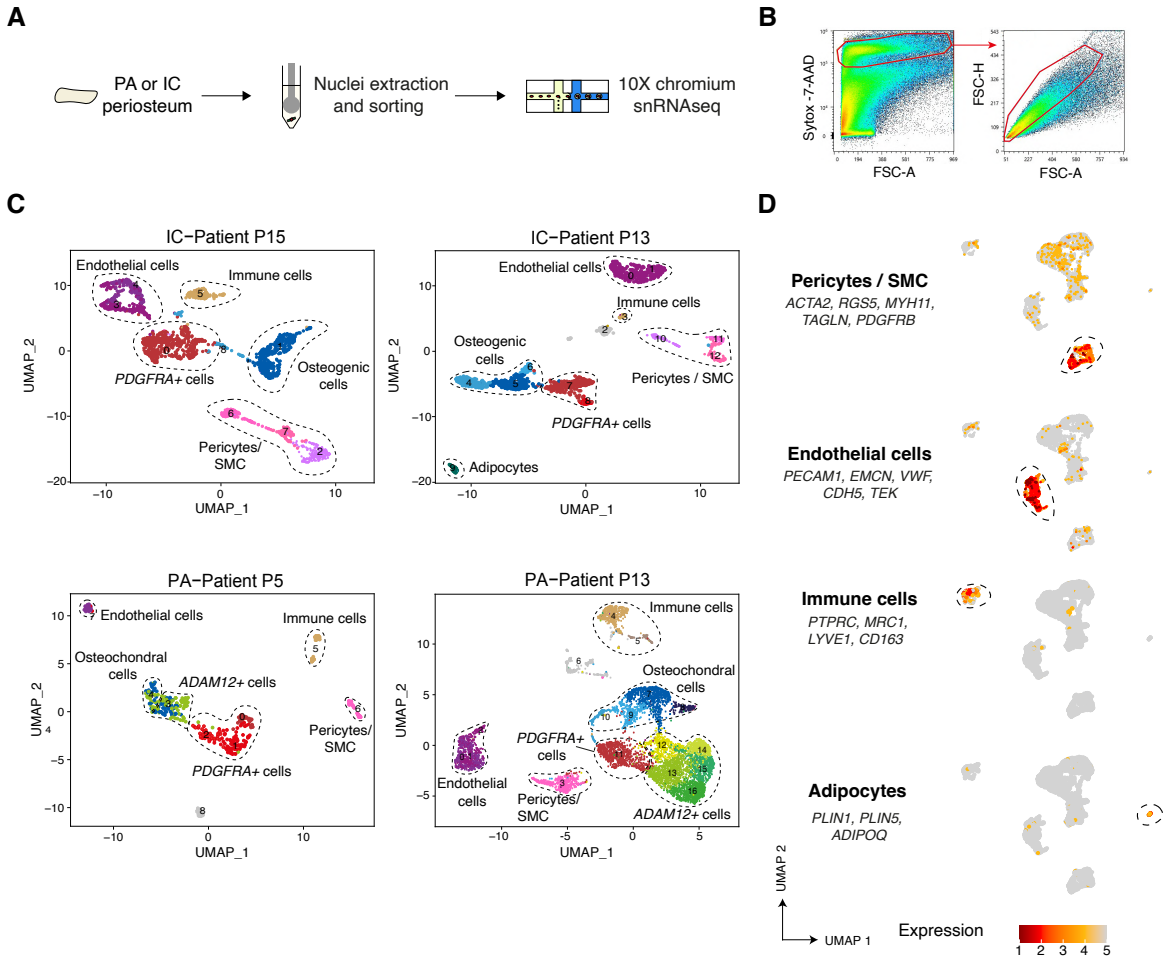

Figure S9: Single nuclei RNAseq analyses of human pathological periosteum

A. Experimental design. Nuclei were extracted from periosteum of IC of P13 and P15 and periosteum of PA site of P13 and P15, sorted and processed for snRNAseq. **B.** Sorting strategy of nuclei stained with Sytox-7AAD for snRNAseq. Sorted nuclei are delimited by a red box. **C.** UMAP projection of the four independent datasets. Cell populations are delimited by dashed lines. **D.** Feature plots of the lineage score of pericytes / smooth muscle cells (SMC), endothelial cells, immune cells, and adipocytes in the integrated datasets.

Figure S10

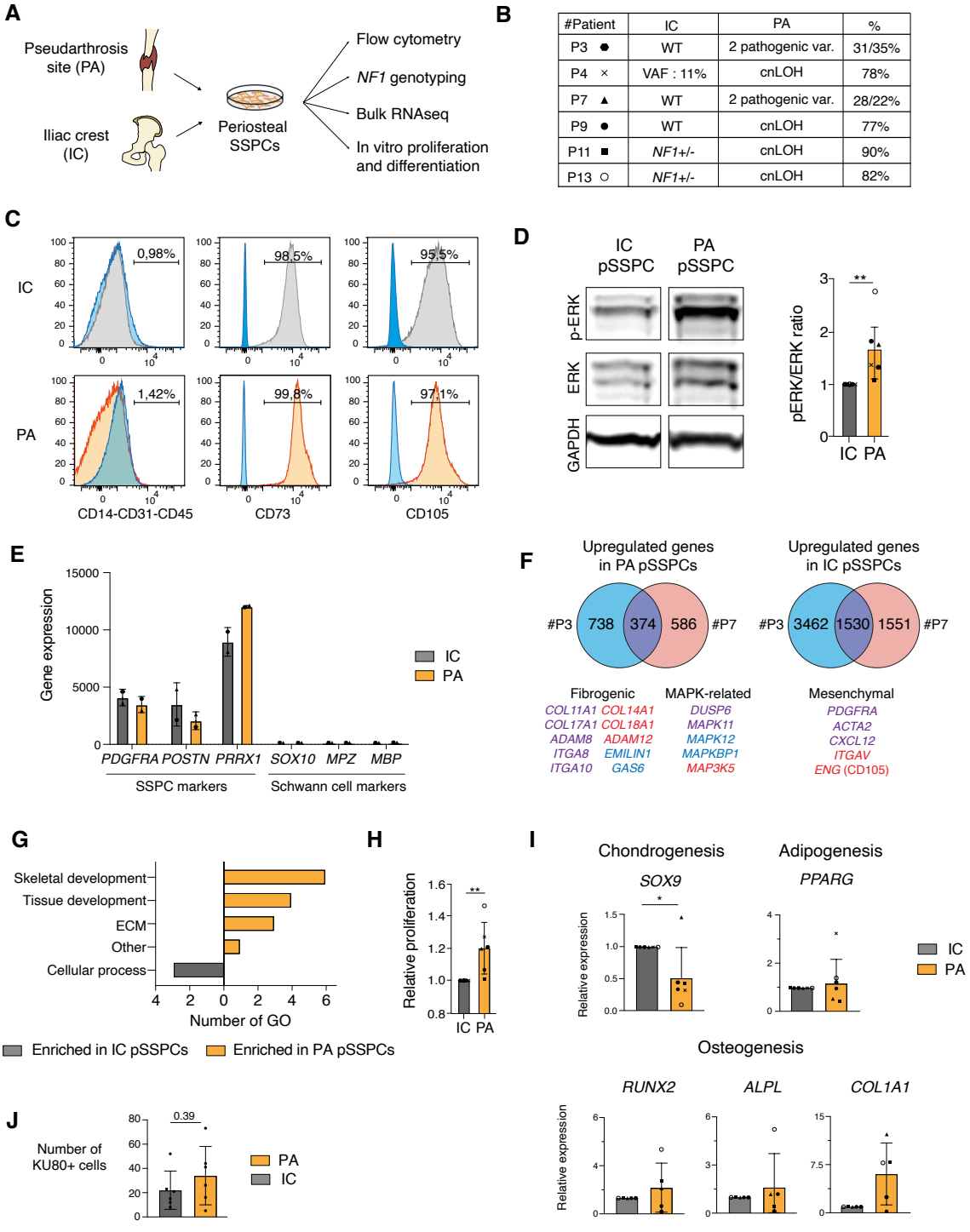

Figure S10: Genotyping, pro-fibrotic profile and differentiation potentials of human SSPCs from pathological periosteum

A. Experimental design. Periosteum collected at the pseudarthrosis (PA) site or iliac crest (IC) was cultured to isolate periosteal skeletal stem/progenitor cells (pSSPCs) used to perform flow cytometry, *NF1* genotyping and in vitro analyses. **B.** *NF1* sequencing of pSSPCs from IC and PA site of patients

P3, P4, P7, P9, P11 and P13, used for in vitro characterization. **C.** Flow cytometry analyses of cultured pSSPCs from PA site and IC, showing that they express mesenchymal markers (CD73, CD105) but not immune and endothelial markers (CD14, CD31, CD45). Samples are in orange/grey and Fluorescent Minus One (FMO) controls are in blue. **D.** Increased MAPK pathway activation in pSSPCs from PA site compared to pSSPCs from IC measured by the ratio of pERK/ERK on Western Blot (n=6 per group, each symbol represents a patient from Fig. S10B). **E.** Expression of SSPC/fibrogenic cell markers (*PDGFRA, POSTN, PRRX1*) and Schwann cell markers (*SOX10, MBP, MPZ*), showing the absence of Schwann cells in the primary pSSPC cultures. **F.** Periosteal SSPCs from IC and PA were processed for bulk RNA sequencing (top). Venn diagrams and list of genes upregulated in PA pSSPCs (left) and IC pSSPCs (right) in only patient P3 (blue), only patient P7 (red) and both patients (purple). **G.** Gene ontology (GO) of the upregulated genes in pSSPCs from IC (left, grey) and PA site (right, orange) of patients P3 and P7. **H.** Increased in vitro proliferation of PA pSSPCs compared to IC pSSPCs (n=6 patients per group). **I.** Relative expression of *SOX9, PPARG*, *RUNX2, ALPL,* and *COL1A1* by in vitro differentiated pSSPCs from IC and PA into the chondrogenic, adipogenic and osteogenic lineage respectively. (n=5-6 patients per group). **J.** Number of KU80+ cells per section in the callus of immunodeficient mice grafted with human IC or PA-derived pSSPCs, showing similar contribution of both IC and PA grafted cells to the fracture callus. p-value: * $p < 0.05$, ** $p < 0.01$. ECM: Extracellular matrix. VAF: variant allele frequency. Var.: variant.

Figure S11

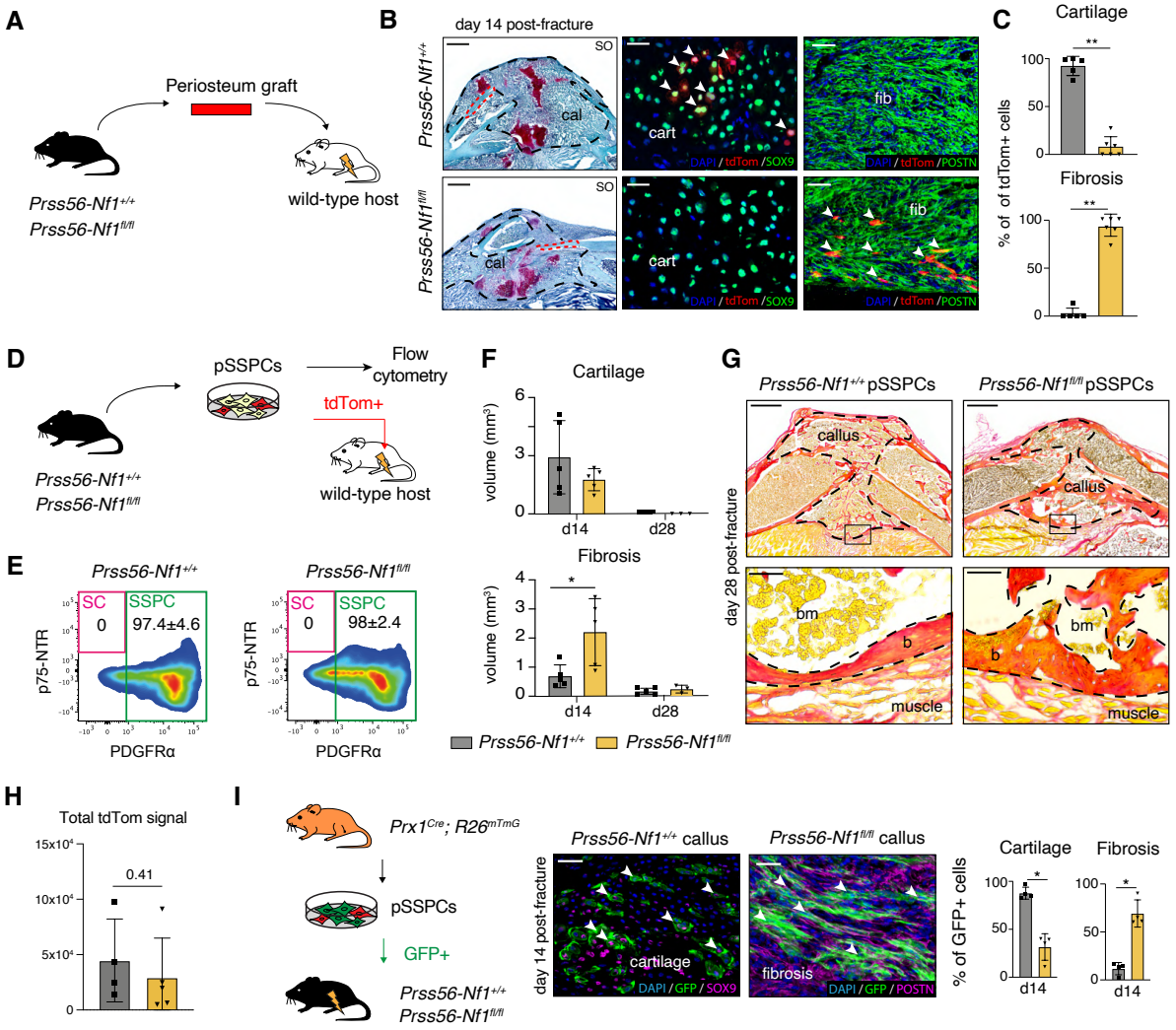

Figure S11: Pro-fibrotic potential of *Prss56-Nf1* KO periosteum and periosteal SSPCs

A. Experimental design. Periosteum was isolated from *Prss56-Nf1*$^{+/+}$ or *Prss56-Nf1*$^{fl/fl}$ mice and transplanted at the fracture site of a wild-type host. **B.** Representative Safranin'O (SO) staining of longitudinal day 14 post-fracture callus section of wild-type host grafted with *Prss56-Nf1*$^{+/+}$ or *Prss56-Nf1*$^{fl/fl}$ periosteum (graft is delimited by red dashed line). Representative images of the contribution of tdTom+ cells showing that cells from *Prss56-Nf1*$^{+/+}$ periosteum are located in cartilage (labelled by SOX9) and cells from *Prss56-Nf1*$^{fl/fl}$ periosteum are located in fibrosis (labelled by POSTN). **C.** Percentage of the contribution of control and mutant tdTom+ cells to cartilage and fibrosis (n= 5-6 per group). **D.** Experimental design. Cultured tdTom^{+} periosteal skeletal stem/progenitor cells (pSSPCs) were isolated from *Prss56-Nf1*$^{+/+}$ or *Prss56-Nf1*$^{fl/fl}$ mice and analyzed by flow cytometry or transplanted at the fracture site of a wild-type host. **E.** Flow cytometry analyses of *Prss56-Nf1*$^{+/+}$ or *Prss56-Nf1*$^{fl/fl}$ cultured periosteal cells showing that cultured tdTom^{+} are PDGFRα+ SSPCs (97.4% ± 4.6 for *Prss56-*

Nf1$^{+/+}$ mice and 98 % ± 2.4 for *Prss56-Nf1*$^{fl/fl}$ mice) (n= 5-6 per group). **F.** Histomorphometric quantification of the volume of cartilage and fibrosis at days 14 and 28 post-fracture of wild-type mice grafted with pSSPCs from *Prss56-Nf1*$^{+/+}$ or *Prss56-Nf1*$^{fl/fl}$ mice (n= 3-5 per group). **G.** Representative Picrosirius (PS) staining of sections of day 28 post-fracture callus grafted with pSSPCs from *Prss56-Nf1*$^{+/+}$or *Prss56-Nf1*$^{fl/fl}$ mice showing bone bridging in both groups. (n = 3 – 5 mice per group). **H.** Total tdTom signal in the callus of wild type grafted with *Prss56-Nf1*$^{+/+}$ or *Prss56-Nf1*$^{fl/fl}$ pSSPCs, showing similar contribution of *Prss56-Nf1*$^{+/+}$ or *Prss56-Nf1*$^{fl/fl}$ grafted cells to the fracture callus. **I.** Left: Experimental design. Cultured GFP^{+} pSSPCs were isolated from *Prx1*^{Cre}*; R26*^{mTmG} mice and transplanted at the fracture site of *Prss56-Nf1*$^{+/+}$ control or *Prss56-Nf1*$^{fl/fl}$ mutant hosts. Middle: Representative images of the contribution of GFP+ pSSPCs to cartilage (labelled by SOX9) in *Prss56-Nf1*$^{+/+}$ hosts and to fibrosis (labelled by POSTN) in *Prss56-Nf1*$^{fl/fl}$ hosts. Right: Percentage of the contribution of grafted GFP+ pSSPCs to cartilage and fibrosis in *Prss56-Nf1*$^{+/+}$ and *Prss56-Nf1* $^{fl/fl}$ hosts (n=4 mice per group). p-values: * $p < 0.05$, ** $p < 0.005$. Scale bars: Low magnification: 1mm. Panel B/H: 100µm. Panel G: High magnification: 200µm.

Figure S12

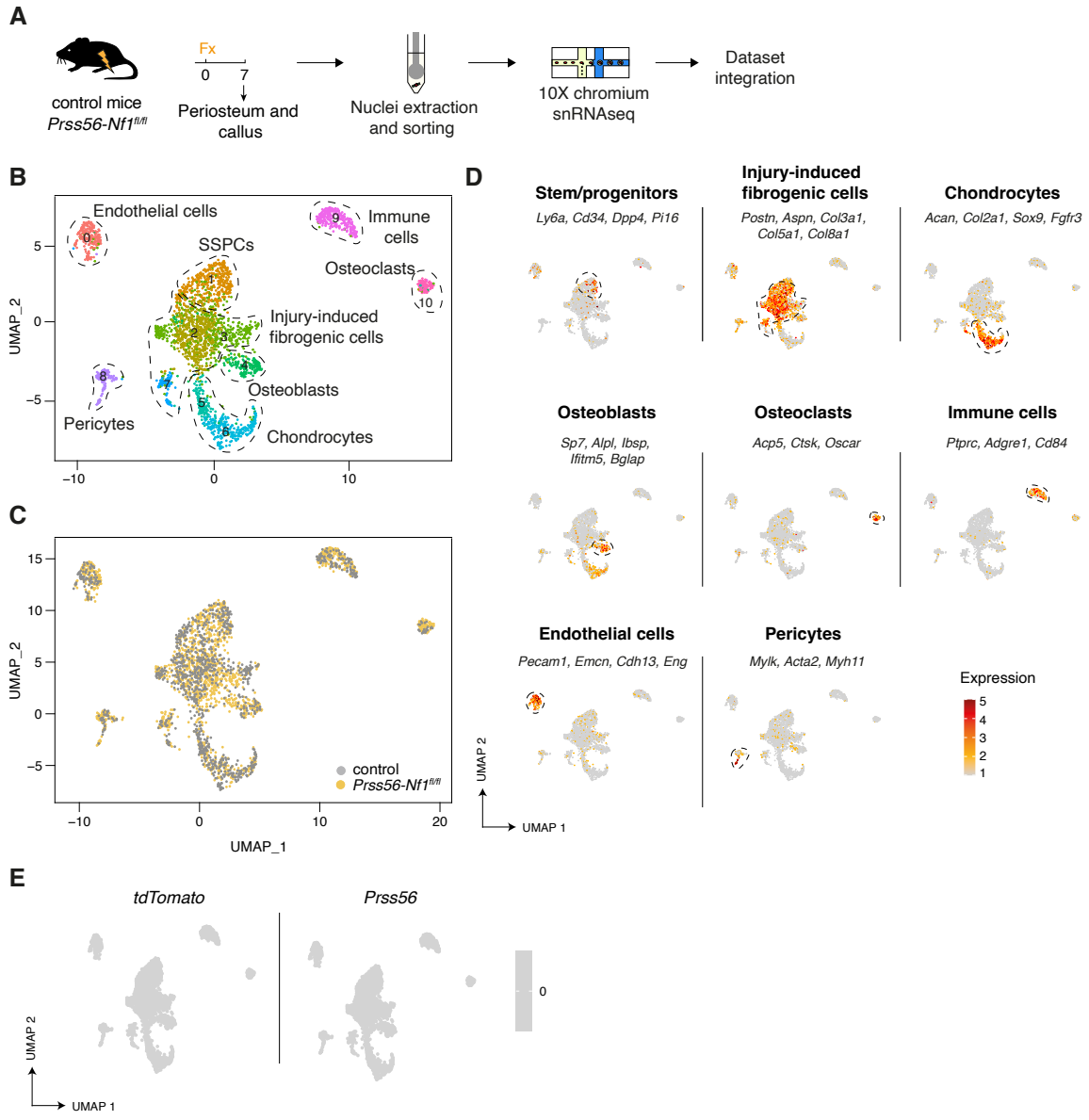

Figure S12: Integration of snRNAseq datasets from day 7 post-fracture callus of control and *Prss56-Nf1$^{fl/fl}$* mice.

A. Experimental design. Nuclei were extracted from the periosteum and callus of control and *Prss56-Nf1$^{fl/fl}$* mice at day 7 post-fracture and processed for single-nuclei RNAseq. **B-C.** UMAP projection of color-coded clustering (B) and color-coded sampling (C) of the integration of the control and *Prss56-Nf1$^{fl/fl}$* day 7 post-fracture datasets. 8 populations are identified (delimited by black dashed lines): pericytes, endothelial cells, skeletal/stem progenitor cells (SSPCs), fibrogenic cells, chondrocytes, osteoblasts, immune cells and osteoclasts. **D.** Lineage score of the different cell populations identified. **E.** Feature plots of *tdTomato* and *Prss56* expression.

Figure S13

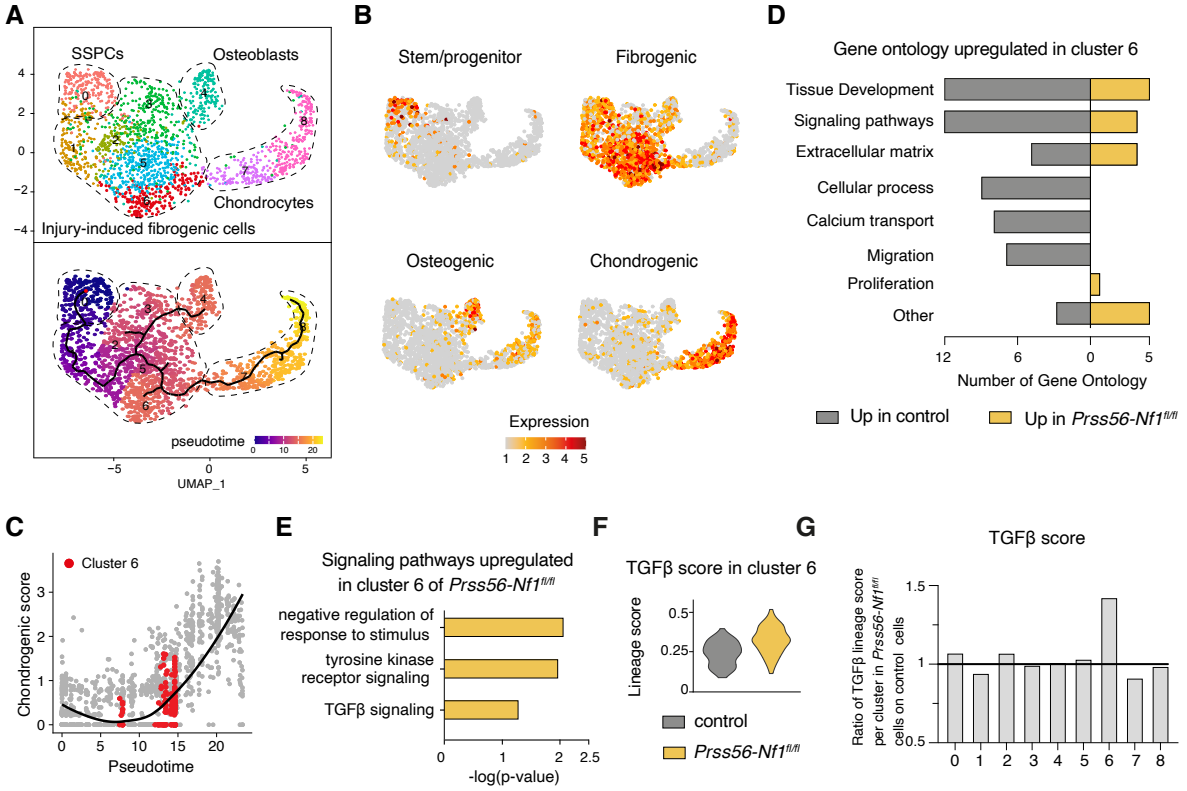

Figure S13: Increased TGFβ signaling in IIFCs from *Prss56-Nf1* KO calluses.

A. UMAP projection of clustering and pseudotime trajectory of the subset of SSPCs, injury-induced fibrogenic, chondrogenic and osteogenic cells from the integration of day 7 post-fracture control and *Prss56-Nf1*$^{fl/fl}$ datasets. **B**. Lineage score of the stem/progenitor, fibrogenic, osteogenic and chondrogenic populations in the subset of the integration of control and *Prss56-Nf1*$^{fl/fl}$ day 7 post-fracture datasets. **C.** Scatter plot of the chondrogenic score along pseudotime. Cells from cluster 6 are in red. **D.** Gene Ontology of upregulated genes in cluster 6 of control (grey) and *Prss56-Nf1*$^{fl/fl}$ (yellow) datasets. **E.** Gene Ontology of upregulated genes in cluster 6 of *Prss56-Nf1*$^{fl/fl}$ dataset in "Signaling pathways" category. **F.** TGFβ score in cluster 6 from control and *Prss56-Nf1*$^{fl/fl}$ datasets. **G.** Ratio of TGFβ lineage score per cluster in *Prss56-Nf1*$^{fl/fl}$ cells on control cells in the subset of pSSPCs, fibrogenic, chondrogenic and osteogenic cells.

Figure S14

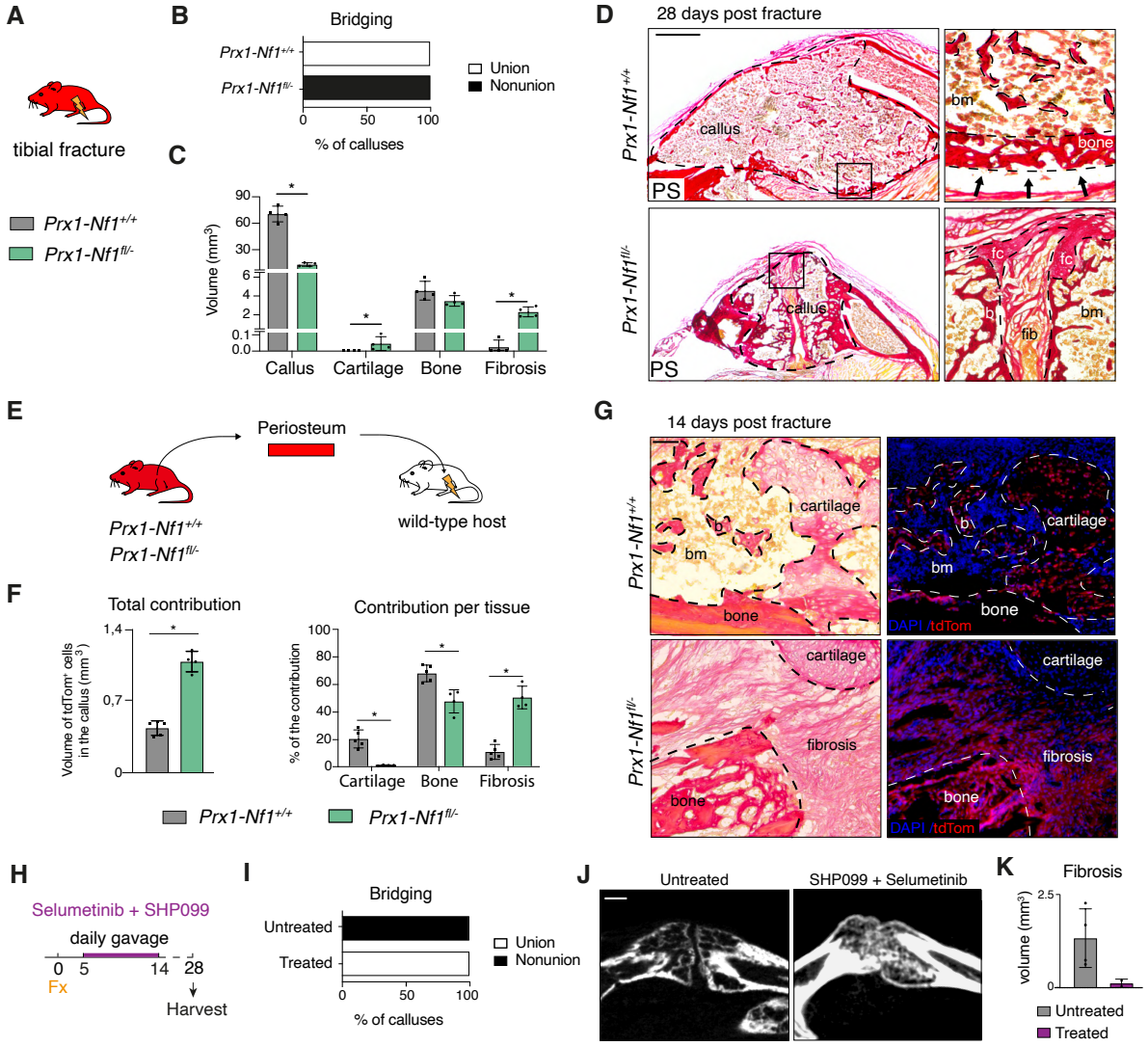

Figure S14: Combined MEK/SHP2 inhibition prevents fracture nonunion in *Prx1-Nf1* KO mice.

A. Experimental design. Tibial fracture was induced to *Prx1*^{Cre}*; R26*^{tdTom}*; Nf1*$^{fl/-}$ (*Prx1-Nf1*$^{fl/-}$) mutant and *Prx1*^{Cre}*; R26*^{tdTom}*; Nf1*$^{+/+}$ (*Prx1-Nf1*$^{+/+}$) control mice. **B.** Percentage of calluses from *Prx1-Nf1*$^{+/+}$ and *Prx1-Nf1*$^{fl/-}$ mice showing bone union (white), semi-union (grey) or nonunion (black) at day 28 post-fracture (n=4 mice per group). **C.** Histomorphometric quantification of the volume of callus, cartilage, bone and fibrosis at day 28 post-fracture in *Prx1-Nf1*$^{+/+}$ and *Prx1-Nf1*$^{fl/-}$ mice (n=4 mice per group). **D.** Representative callus sections of *Prx1-Nf1*$^{+/+}$ and *Prx1-Nf1*$^{fl/-}$ mice at 28 days post-fracture stained with Picrosirius (PS) and high magnification of callus periphery showing bone bridging in *Prx1-Nf1*$^{+/+}$ control mice and presence of fibrosis in *Prx1-Nf1*$^{fl/-}$ mutant mice. **E.** Experimental design. Periosteum from *Prx1-Nf1*$^{+/+}$ and *Prx1-Nf1*$^{fl/-}$ mice was grafted at the fracture site of WT hosts. **F.** Total contribution and

percentage of tissue contribution from the grafted periosteum of *Prx1-Nf1*$^{+/+}$ and *Prx1-Nf1*$^{fl/-}$ mice (n=3-5 per group). **G.** Representative callus section showing that tdTom+ cells from the control graft contributed to cartilage and bone while tdTom+ cells from *Prx1-Nf1*$^{fl/-}$ mice contributed to bone and fibrosis. **H.** Experimental design. *Prx1-Nf1*$^{fl/-}$ mutant mice were treated with daily gavage of Selumetinib and SHP099 from days 5 to 14 post-fracture. **I.** Percentage of calluses from treated and untreated *Prx1-Nf1*$^{fl/-}$ mice showing bone union (white), semi-union (grey) or nonunion (black) at day 28 post-fracture (n=2-4 mice per group). **J.** Representative microCT scan of treated and untreated *Prx1-Nf1*$^{fl/-}$ mice at 28 days post-fracture. **K.** Volume of fibrosis in the callus of treated and untreated *Prx1-Nf1*$^{fl/-}$ mice at 28 days post-fracture (n=2-4 mice per group). p-value: * $p < 0.05$. Scale bars: Panel A/J: 1mm, Panel G: 250μm.

#ID	Blood	2nd hit	VAF periost.	VAF Fibrous tis.
P4	VAF:38%	cnLOH	61%	23%#
P5	*NF1*+/-	Point PV	32%	2%
P9	WT	cnLOH	77%	7%

Table S2: *NF1* genotyping in blood, PA periosteum and fibrous tissue of patients P4, P5 and P9, showing absence of a 2nd mutational event in fibrous tissue of P4 and low level of a 2nd mutational event in fibrous tissue of P5 and P9.

Antibody type	Use	Antigen	Reference	Dilution
Primary	IF	Rabbit polyclonal to human CD90 (THY1)	555596, BD Biosciences	1:200
Primary	IF	Mouse monoclonal to human Alpha-Smooth Muscle	50-9760-82, Invitrogen	1:200
Primary	IF	Mouse monoclonal to human PECAM1	M0823, Dako	1:200
Primary	IF	Mouse monoclonal to human CD68	M0814, Dako	1:200
Primary	IF	Rabbit polyclonal to mouse and human phospho-ERK	9101S, Ozyme	1:200
Primary	IF	Rabbit polyclonal to mouse phosho-SMAD2	3101, Cell signaling	1:200
Primary	IF	Rabbit monoclonal to mouse SOX9	ab185230, Abcam	1:1000
Primary	IF	Rabbit polyclonal to mouse Osterix/Sp7	ab22552, Abcam	1:200
Primary	IF	Goat polyclonal to mouse Periostin	AF2955, R&D Systems	1:400
Primary	IF	Rabbit monoclonal to human KU80	2180T, Ozyme	1:200
Primary	IF	Goat polyclonal to mouse PDGFRα	AF1062, RD Systems	1:200
Primary	IF	Rabbit monoclonal to mouse SOX10	BSB2583, BioSB	1:200
Primary	IF	Rabbit polyclonal to mouse Tyrosine Hydroxylase	AB152, Merck	1:400
Primary	IF	Rabbit polyclonal to mouse SOX2	ab97959, Abcam	1:200
Primary	IF	Rabbit monoclonal to mouse MBP	HL1033, GeneTex	1:200
Primary	IF	Rabbit polyclonal to mouse Collagen II	ab34712, Abcam	1:200
Primary	IF	Rabbit polyclonal to mouse Collagen X	ab58632, Abcam	1:200
Primary	IF	Rat monoclonal to mouse CD68	137002, BioLegend	1:200
Primary	IF	Goat polyclonal to mouse PECAM1	AF3628, Biotechne	1:100
Secondary	IF	FITC - Goat anti mouse Ig	115-095-166, Jackson ImmunoResearch	1:200
Secondary	IF	Alexa Fluor 647 goat anti rabbit Ig	A-21245, Invitrogen	1:200
Secondary	IF	Alexa Fluor 488 goat anti rabbit Ig	A-11034, Invitrogen	1:1000
Secondary	IF	Alexa Fluor 647 donkey anti goat Ig	A-21447, Invitrogen	1:1000
Secondary	IF	Alexa Fluor 488 donkey anti goat Ig	A11055, Invitrogen	1:200
Primary	FC	anti-human CD31-PeCy7	563651, BD Biosciences	1:400
Primary	FC	anti-human CD45-PeCy7	60915, BD Biosciences	1:400

Primary	FC	anti-human CD14-PeCy7	557742, BD Biosciences	1:400
Primary	FC	anti-human p75-NTR-BV510	563451, BD Biosciences	1:200
Primary	FC	anti-human CD140a-PE	556002, BD Biosciences	1:200
Primary	FC	anti-human CD31-FITC	557508, BD Biosciences	1:200
Primary	FC	anti-human CD73-BV711	742634, BD Biosciences	1:200
Primary	FC	anti-human CD105-APC	562408, BD Biosciences	1:200
Primary	FC	anti-mouse CD31-PeCy7	561410, BD Biosciences	1:400
Primary	FC	anti-mouse CD45- PeCy7	552848, BD Bioscience	1:400
Primary	FC	anti-mouse CD11b- PeCy7	552850, BD Biosciences	1:400
Primary	FC	anti-mouse Sca1-BV605	740450, BD Biosciences	1:200
Primary	FC	anti-mouse CD140A-BV711	740740, BD Biosciences	1:200
Primary	FC	anti-mouse p75-NGFR-FITC	130-110-115, Milteny	1:200
Primary	WB	Rabbit monoclonal to human p44 MAPK (ERK1)	9101, Cell signaling	1:1000
Primary	WB	Mouse monoclonal to human GAPDH	sc-47724, Santa Cruz	1:5000
Primary	WB	Rabbit polyclonal to human p44/42 MAPK (Erk1/2)	9102, Cell signaling	1:1000
Secondary	WB	Mouse IgG HRP Linked Whole Ab	GENXA931-1ML, Merck	1:2500
Secondary	WB	Rabbit IgG HRP Linked F(ab')2	GENA9340-1ML, Merck	1:2500

Table S3: List of antibodies used for this study. IF: immunofluorescence. FC: Flow cytometry. WB: Western Blot

Gene	Primers	
TBP	5’ TGCACAGGAGCCAAGAGTGAA 3’	5’ CACATCACAGCTCCCCACCA 3’
SOX9	5' GCCACGGAGCAGACGCACAT 3'	5' CCCTGGGATTGCCCCGAGT 3'
RUNX2	5' CGGAATGCCTCTGCTGTTATGAA 3'	5' ACTCTTGCCTCGTCCACTCCG 3'
COL1A1	5' CCTCCGGCTCCTGCTCCTCTT 3'	5' GGCAGTTCTTGGTCTCGTCACA 3'
ALPL	5' AAGAAGCCCTTCACTGCCATCC 3'	5' AGTTGTTGTGAGCATAGTCCACCATG 3'
PPARG	5' GCCACGGAGCAGACGCACAT 3'	5' CCCTGGGATTGCCCCGAGT 3'
Tgfb1	5' ACTGGAGTTGTACGGCAGTG 3'	5' GGCTGATCCCGTTGATTTCC 3'
PDGFRA	5' CATTTACATCTATGTGCCAGACCCA 3'	5' ATGGCAGAATCATCATCCTCCAC 3'

Table S4: List of qPCR primers used for this study.

Lineage	Genes
Skeletal stem/progenitor cells (SSPC)	*Ly6a, Cd34, Dpp4, Pi16*
Fibrogenic cells	*Postn, Aspn, Col3a1, Col5a1, Col8a1*
Chondrocytes	*Acan, Col2a1, Sox9, Col9a1*
Osteoblasts	*Sp7, Alpl, Ibsp, Bglap*
Endothelial cells	*Pecam1, Emcn, Cdh13, Eng*
Pericytes	*Mylk, Acta2, Myh11*
Osteoclasts	*Acp5, Ctsk, Oscar*
Immune cells	*Ptprc, Adgre1, Cd84*
Schwann cells	*Mpz, Mbp, Nfasc, Ntng1*
Adipocytes	*Pparg, Lipe, Plin1*
MAPK pathway activation	*Epgn , Gpr39 , Mst1r , Zeb2 , Pdgfc , Nek10 , Rps3 , Fgd4 , Nox4 , Bcl10 , Ccr7 , Flt1 , Fgfr1 , Fgf2 , Fgf1 , Fgd2 , Pdcd10 , Fzd10 , Syk , Ghr , Ceacam1 , Pik3r5 , Erbb2 , Src , Egf , Edn3 , Ror2 , Tnf , Pdgfd , Adam8 , Dusp19 , Mif , Kitl , Tlr9 , Irak1 , Igh-7 , Tlr6 , Map3k13 , Tnfrsf11a , Ntrk3 , Erp29 , Ajuba , Kras , Kit , Ezh2 , Dusp6 , Ptprc , Ptpn1 , Pdgfrb , Pdgfb , Pdgfa , Dab2ip , Map2k4 , Map2k6 , Ccl19 , Vangl2 , Fgf18 , Lrrk2 , Magi3 , Dkk1 , Pik3cg , Il34 , Ilk , Drd4 , Adra2a , Ern2 , Adam9 , Pak1 , P2rx7 , Cd40 , Cd24a , Wnt5a , Dvl2 , Tdgf1 , Csk , Tgfb1 , Tgfa , Arhgef5 , Htr2b , Axin1 , Egfr , Htr2a , Map4k2 , Map3k12 , Map3k11 , Map3k10 , Map3k7 , Tab1 , Map2k5 , Tirap , Taok3 , Mapk8ip3 , Edn1 , Epha4 , Ager , Robo1 , Fcer1a , Map3k4 , Map3k1 , Map2k7 , Nod2 , Tpd52l1 , Sash1 , Tenm1 , Psen1 , Tlr4 , Fzd5 , Traf2 , Fzd4 , Dvl3 , Pik3r6 , Traf6 , Akap13 , Ptk2b , Ntf3 , Prkcd , Tnfsf11 , Fzd8 , Pde5a , Gab1 , Hras , Rasgrp1 , Insr , Il1rn , Il1b*
Cellular response to TGFβ stimulus	*Sox9, Sox6, Sox5, Trp53, Eid2, Apaf1, Cited2, Bmp2, Crk, Skil, Tgfbr2, Tgfb3, Tgfb1, Creb1, Col1a2, Col4a2, Col3a1, Spi1, Ccl2, Dab2, Dnmt1, Dlx1, Appl1, Tab1, Mapk7, Ptprk, Mstn, Eng, Fut8, Scx, Zyx, Map3k7, Map3k1, Smad1, Itga8, Cav1, Acvr1, Npnt, Onecut2, Dcp1a, Stk16, Pdcd5, Ppargc1a, Flcn, Mir145b, Acvr1c, Gcnt2, Actr3, Parp1, Fermt2, Usp9x, Zmiz1, Smad3, Yes1, Cav2, Gdnf, Appl2, Cilp, Jun, Zfyve9, Itgb1, Dbn1, Smad9, Onecut1, Hyal2, Nlk, Ankrd1, Dusp22, Igf1r, Arrb2, Mef2c, Cldn5, Crkl, Mir21a, Mir192, Mir155, Mir145a, Usp15, Hpgd, Acvrl1, Glg1, Ltbp4, Lpxn, Nrros, Smad7, Itgb5, Itgb6, Pxn, Nos3, Nodal, Serpine1, Amhr2, Cdh5, Pml, Tgfbr3, Xcl1, Bmp8a, Twsg1, Foxh1, Nr3c1, Fyn, Mtmr4, Stat3, Epb41l5, Fos, Ptk2, Zfp36l1, Zfp36l2, Wfikkn2, Ovol2, Itgb8, Bmp8b, Ppm1a, Runx1, Smad2, Lrrc32, Sirt1, Bambi, Tgfbr3l, Akr1c18, Mir143, Smad5, Cited1, Smad6, Src, Tgfb2, Tgfbr1, Smad4, Adam9, Hipk2, Wwox*

Table S5: Lists of genes used for lineage score analyses of murine snRNAseq.

Lineage	Genes
SSPC/Fibroblast	*DPP4, NT5E, PRRX1, GSN*
Fibrotic score	*POSTN, ASPN, COL1A1, COL1A2, COL6A3, COL3A1*
Chondrogenic score	*ACAN, FGFR3*
Osteogenic score	*ALPL, RUNX2*
Endothelial cells	*PECAM1, EMCN, VWF, CDH5, TEK*
Pericytes / SMC	*ACTA2, RGS5, MYH11, TAGLN, PDGFRB*
Immune cells	*PTPRC, MRC1, LYVE1, CD163*
MAPK pathway activation	*EDN1, TAOK3, HIPK2, RASGRP1, GADD45G, MT3, BANK1, GPR55, FERMT2, PTPN22, LAMTOR2, CCL3, MAPKBP1, CD40, ZC3H12A, CDH2, VEGFA, PSEN1, LPAR3, IL6, FGF1, KDR, FZD4, ALK, FZD10, FLT4, PYCARD, FGF20, EZH2, NOX1, CD36, PRMT1, CCL3L1, MYD88, CIB1, TIRAP, SOX2, FGF10, FZD5, ROCK1, TAOK2, DNAJC27, CD74, ADAM9, RYK, HAND2, TREM2, DENND2B, PTPRC, PRKD2, TGFBR1, ERBB4, FLT3, ALKAL2, TRAF5, DOK4, DKK1, SCIMP, GPER1, FZD8, CRKL, CRK, HGF, NODAL, FGF23, STK3, PDGFD, MAP2K5, PAK1, ERN2, PDE6H, WWC1, PROK1, FFAR4, P2RY6, TRAF3, RAMP3, MIF, EDN3, GLIPR2, HMGB1, AXIN1, CCL16, TLR3, CCL25, SPHK1, AVPI1, SRC, CRACR2A, NENF, FGG, FGB, FGA, APOE, ITGA1, KLHDC10, PDGFRB, IGFBP6, GPR37, TP73, MID1, PDGFA, GADD45A, RAF1, GRM1, CCL22, CCL19, GDF15, GFRAL, ABCA7, TRAF7, LGALS9, CSK, NPY, CCL24, WNT5A, KSR1, NOD2, ALOX15, MAP2K2, NTRK1, CX3CL1, HLA-DRB1, NOTCH1, NEK10, WNT7B, CHI3L1, DOK6, SH3RF3, EPGN, SH3RF2, GNAI2, RB1CC1, CSPG4, PDGFRA, GPBAR1, CCL11, SDCBP, MAP3K4, LTBR, STK25, NPNT, SSTR4, MAP4K1, DUSP19, SYK, FRS2, CXCL17, NPY5R, MADD, TAB1, KISS1, GATA4, XCL1, RAP1B,HAVCR2, CAV2, S100A7,IRAK1, IQGAP1, AGER, TGFB2, RIPK1, ADAM8, NCF1, PLA2G2A, C1QTNF1, GDF6, SYT14P1, CD4, TRPV4, IQGAP3, CASR, LEP, OPRK1, EDA2R, RELL1, PELI2, CCL20, MAP3K3, DIXDC1, ROR1, WNT7A, NTF3, NPTN, ARRB2, PRDX2, AVPR1B, P2RY1, MAGED1, CALCR, RAP1A,NOTCH2, FGF19, TNIK, ALOX12B, DIRAS2, LAMTOR1, SLC30A10, CCL26, CARD9, DAB2IP, C5AR2, MAP3K11, CARTPT, CSF1R, NDST1, PTPN11, HCRTR1, SOD1, EFNA1, NAIP, MST1R, MFHAS1, CCL4L1, ERN1, TGFB3, LAMTOR3, GPR183, CCR7, CCR1, MARCO, STK39, NTRK3, IL11, TLR6,SPRY2 ANKRD6, ARRB1, GPNMB, MAP2K6, MAP3K7, MAPK3, MOS, EGFR, ABL1, PPIA, ROBO1, PRKCA, SEMA7A, ACTA2, BIRC7, NPSR1, GHR, MAP3K13, XDH, KIT, DOK5, CCN2, ARL6IP5, ADRB2, MBIP, GAREM1, DHX33, IL34, DSTYK, EIF2AK2, PDE8A, FCRL3, XIAP, TLR9, SORBS3, CDC42, PLA2G5, THBS1, SHC2, BMP4, BMP2, FGF21, PIK3R6, IGFBP4, ICAM1, SPAG9, SHC1, FGFR3, FLT1, SPI1, NDRG4, RIPK2, FGFR4, BCAR3, GADD45B, MEF2C, APELA, TENM1, PDGFC, RASSF2, RET, EPHA4, MMP8, GSDME, FGF2, MAP3K10, AJUBA, TBX1, CCL14, NTRK2, IAPP, CCL1, TPD52L1, TNFAIP8L3, DDR2, JUN, TNF, ANGPT1, HTR2B, GRM5, KLB, HTR2C, TGFB1, TGFA, EGF, CD27, PDGFB, HRAS, CDON, KL, PIK3R5, P2RX7,*

	RIT2, TRAF6, FGFR1, ADRA2B, PTPN1, DRD4, RAPGEF2, PRXL2C, CCL17, KITLG, PLCG2, PIK3CG, HTR2A,PHB2,PRKCZ, FGF18, ARHGAP8, DVL3, PDE5A, ALKAL1, NELFE, TPBG, CHRNA7, SASH1, INAVA, PDE6G, MINK1, TMEM106A, CCL7, CCL8, TAOK1, IGF2, FGFR2, IGF1R, CDK10, INS, LPAR1, LRRK2, INSR, GCG, C5AR1, GCNT2, CCL13, GH1, FCGR2B, MAP3K5, ADCYAP1, EPO, IL1B, IL1A, ELANE, F2RL1, FGF8, CCL21, CCL4, TLR4, S100A12, CD81, CTNNB1, UNC5CL, DRD2, NRG1, ADRB3,THPO, ROCK2, GRM4, TNFRSF11A, AR, FZD7, WNT16, GHRL, NOD1, CCL15, ADORA1, IGFBP3, EPHA8, SEMA3A, XCL2, RELL2, MAPK8IP3,BRAF, MAP3K12, MAP4K2, LIF, AKAP13, MAP2K3, ERBB2,MAPK8IP1,ZNF622, ITGB3,CD44, CCL5, CCL2, PJA2,LILRA5, SLAMF1, PDCD10, BMPER, PRKCE, TRAF4, GAS6, JAK2, NOX4, IL26, AKAP12, PLCB1, APP, DIRAS1, EDAR, PTK2B, TRIM5, IGF1, SEMA4C, MAP2K4, ARHGEF5, MYDGF, FBXW7, CAVIN3,F2R, OSM, ACKR3, ADRA1D, CFLAR, TNFSF11, NRP1, OPRM1, ADRA1B, PLA2G1B, ADRA1A, MAP2K7, FSHR, ROR2, MAPK8IP2, TDGF1, JCAD, SERPINF2, PLCE1, FGF4, ADRA2C, TEK, GPR37L1, MAP2K1, OR2AT4, TNFRSF19, DUSP22, TRAF2, PTPRJ, DDT, ERP29, TRAF1, FPR2, CD24, PTEN, CCL18, CCL23, ADRA2A, DVL2, PHB1, FGD2, SH3RF1, NECAB2, LAPTM5, INHBA, RPS3, MTURN
Cellular response to TGFβ stimulus	*ABL1, ACVR1, ACVRL1, ADAM9, AMHR2, ANKRD1, APAF1, APOA1, APPL1, APPL2, ARG1, ARRB2, BAMBI, BMPR1A, CAV1, CAV2, CDH5, CDKN2B, CHST11, CILP, CITED1, CITED2, CLDN1, CLDN5, CLEC3B, COL1A1, COL1A2, COL3A1, COL4A2, CRK, CRKL, CTSK, CX3CR1, DAB2, DCSTAMP, DDR2, DLX1, DUSP22, EDN1, EID2, ENG, EPB41L5, FBN1, FERMT2, FGFR2, FLCN, FMOD, FNTA, FOXH1, FSHB, FURIN, FUT8, FYN, GCNT2, GDF10, GDF15, GDF5, GDF9, GLG1, HDAC2, HIPK2, HPGD, HYAL2, ID1, IGF1R, ITGA8, ITGB1, ITGB5, ITGB6, ITGB8, LEFTY1, LIMS1, LPXN, LRRC32, LTBP2, LTBP3, LTBP4, MAP3K7, MAPK7, MEF2C, MSTN, MTMR4, NFATC1, NLK, NODAL, NPNT, NR3C1, NRROS, ONECUT1, ONECUT2, OVOL2, PAK2, PARP1, PDCD5, PDE2A, PDE3A, PDGFA, PDGFD, PENK, PML, PPM1A, PSG9, PTK2, PTPRK, PXN, SCX, SFRP1, SIRT1, SKIL, SMAD1, SMAD2, SMAD3, SMAD4, SMAD5, SMAD6, SMAD7, SMAD9, SOX5, SOX6, SOX9, SPI1, SRC, STK16, TAB1, TGFB1, TGFB2, TGFB3, TGFBR1, TGFBR2, TGFBR3, TGFBR3L, TGFBRAP1, TP53, TWSG1, USP15, USP9X, USP9Y, WFIKKN2, WNT10A, WNT2, WNT4, WNT5A, WNT7A, WWOX, XCL1, YES1, ZEB1, ZFP36L1, ZFP36L2, ZFYVE9, ZMIZ1, ZMIZ2, ZYX*

Table S6: Lists of genes used for lineage score in analyses of human snRNAseq.

References

57. E. Pasmant, B. Parfait, A. Luscan, P. Goussard, A. Briand-Suleau, I. Laurendeau, C. Fouveaut, C. Leroy, A. Montadert, P. Wolkenstein, M. Vidaud, D. Vidaud, Neurofibromatosis type 1 molecular diagnosis: what can NGS do for you when you have a large gene with loss of function mutations? *Eur J Hum Genet* 23, 596–601 (2015).

58. A. Sabbagh, E. Pasmant, A. Imbard, A. Luscan, M. Soares, H. Blanché, I. Laurendeau, S. Ferkal, M. Vidaud, S. Pinson, C. Bellanné-Chantelot, D. Vidaud, B. Parfait, P. Wolkenstein, NF1 molecular characterization and neurofibromatosis type I genotype-phenotype correlation: the French experience. *Hum Mutat* 34, 1510–1518 (2013).

59. S. Perrin, A. Julien, O. Duchamp de Lageneste, R. Abou-Khalil, C. Colnot, Mouse Periosteal Cell Culture, in vitro Differentiation, and in vivo Transplantation in Tibial Fractures. *BIO-PROTOCOL* 11 (2021), doi:10.21769/BioProtoc.4107.

60. M. P. Clements, E. Byrne, L. F. Camarillo Guerrero, A.-L. Cattin, L. Zakka, A. Ashraf, J. J. Burden, S. Khadayate, A. C. Lloyd, S. Marguerat, S. Parrinello, The Wound Microenvironment Reprograms Schwann Cells to Invasive Mesenchymal-like Cells to Drive Peripheral Nerve Regeneration. *Neuron* 96, 98-114.e7 (2017).

61. N. van Gastel, S. Torrekens, S. J. Roberts, K. Moermans, J. Schrooten, P. Carmeliet, A. Luttun, F. P. Luyten, G. Carmeliet, Engineering vascularized bone: osteogenic and proangiogenic potential of murine periosteal cells. *Stem Cells* 30, 2460–2471 (2012).

62. M. D. Santos, S. Gioftsidi, S. Backer, L. Machado, F. Relaix, P. Maire, P. Mourikis, Extraction and sequencing of single nuclei from murine skeletal muscles. *STAR Protocols* 2, 100694 (2021).

63. L. G Martelotto, *'Frankenstein' protocol for nuclei isolation from fresh and frozen tissue for snRNAseq v2* (2019; https://www.protocols.io/view/frankenstein-protocol-for-nuclei-isolation-from-f-3fkgjkw).

64. T. Stuart, A. Butler, P. Hoffman, C. Hafemeister, E. Papalexi, W. M. Mauck, Y. Hao, M. Stoeckius, P. Smibert, R. Satija, Comprehensive Integration of Single-Cell Data. *Cell* 177, 1888-1902.e21 (2019).

65. A. Butler, P. Hoffman, P. Smibert, E. Papalexi, R. Satija, Integrating single-cell transcriptomic data across different conditions, technologies, and species. *Nat Biotechnol* 36, 411–420 (2018).

66. I. Korsunsky, N. Millard, J. Fan, K. Slowikowski, F. Zhang, K. Wei, Y. Baglaenko, M. Brenner, P. Loh, S. Raychaudhuri, Fast, sensitive and accurate integration of single-cell data with Harmony. *Nat Methods* 16, 1289–1296 (2019).

67. J. Cao, M. Spielmann, X. Qiu, X. Huang, D. M. Ibrahim, A. J. Hill, F. Zhang, S. Mundlos, L. Christiansen, F. J. Steemers, C. Trapnell, J. Shendure, The single-cell transcriptional landscape of mammalian organogenesis. *Nature* 566, 496–502 (2019).

68. N. H. Kelly, N. P. T. Huynh, F. Guilak, Single cell RNA-sequencing reveals cellular heterogeneity and trajectories of lineage specification during murine embryonic limb development. *Matrix Biology* 89, 1–10 (2020).